Experiment 823
Pure Fermi decay in medium mass nuclei
(G.C. Ball, TRIUMF)

Precise measurements of the intensities for superallowed Fermi $0^+ \rightarrow 0^+$ β decays have provided a demanding test of the CVC hypothesis at the level of 3×10^{-4}. When the value of the vector coupling constant, G_V, obtained from these superallowed decays is combined with the Fermi coupling constant, G_F, for pure leptonic decays it leads to the most precise determination of V_{ud}, the up-down element of the CKM matrix. Since V_{ud} is now by far the most precisely determined CKM matrix element, intense scrutiny has been focused on the small ($\sim$1%) theoretical corrections required to obtain the transition-independent Ft values. Uncertainties in the calculated isospin symmetry breaking corrections can be studied by extending the precision β-decay measurements to heavier ($A \geq 62$, $T_z = 0$) odd-odd nuclei where these corrections are predicted to be much larger [I.S. Towner and J.C. Hardy, Phys Rev. **C66**, 035501 (2002)]. The primary goal of the E823 experimental program is to measure the half-lives and branching ratios for the superallowed β-decay of these radioactive nuclei produced at ISAC. The early measurements focused on ^{74}Rb (see TRIUMF 1999-2002 Annual Reports).

High-precision branching-ratio measurement of the superallowed β-emitter ^{62}Ga

Non-analogue Fermi and Gamow-Teller branches in the superallowed β-decay of ^{62}Ga were investigated recently at ISAC using the 8π spectrometer. The experiment was carried out in December 2004 using a beam of $\sim$1600 ^{62}Ga ions/s produced during the first beam development run with TRILIS. Details of this experiment were reported previously (see TRIUMF 2004–5 Annual Reports). The analysis of these data has been completed. Nineteen gamma-rays emitted following the β-decay of ^{62}Ga were identified, establishing the dominant superallowed branching ratio to be 99.861 ± 0.011%. When this result is combined with recent half-life and Q-value measurements a superallowed *ft* value of 3075.6 ± 1.4 s is obtained for the decay of ^{62}Ga. As shown in Fig. 1(a) this represents the first case in the $A \geq 62$ mass region with an *ft* uncertainty $\leq$0.05%, comparable to the best measured cases among the lighter $N = Z$ nuclei.

After applying the radiative $\delta_R = 1.405(89)$% and isospin symmetry breaking $\delta_C = 1.38(16)$% corrections from I.S. Towner and J.C. Hardy [*ibid*] we obtain Ft = 3075.8 ± 5.7 s for ^{62}Ga, in excellent agreement with CVC as shown in Fig. 1(b). The precision of the Ft value is, however, now limited entirely by the uncertainty in the calculated isospin-symmetry-breaking correction δ_C. The precise experimental *ft* value for ^{62}Ga can be used to test the theoretical calculations of δ_C. In particular, assuming CVC, from the world average Ft = 3074.4(12) s [G. Savard *et al.*, Phys. Rev. Lett. **95**, 10250 (2005)] and the experimental *ft* value for ^{62}Ga we obtain $\delta_C = 1.42(11)$%. The results obtained in this experiment have now been published in PRL [B. Hyland *et al.*, Phys. Rev. Lett. **97**, 102501 (2006)].

This high-precision branching ratio measurement was repeated in December 2005 using a beam of $\sim$5000 ^{62}Ga ions/s which was more than 95% laser ionized. Approximately three times as much data were obtained. The focus of this experiment was to search for the feeding of non-analogue 0^+ levels in ^{62}Zn, which test the "configuration mixing" component, δ_{C1}, of the isospin symmetry breaking correction. Analysis of these data is in progress.

High-precision measurement of the half-life of the superallowed β-emitter ^{62}Ga

Since the uncertainty in the world average half-life of ^{62}Ga, 116.17 ± 0.04 ms, is dominated by a single high-precision measurement (116.19(04) ms [Blank *et al.*, Phys. Rev. **C69** (2004) 015502]) an experiment designed to obtain comparable or higher precision was carried out in December 2005 at GPS1 using the fast tape transport system. Details of this measurement were reported previously [see TRIUMF 2005 Annual Report]. A preliminary analysis of these data has shown that the statistical uncertainty in the ^{62}Ga half-life obtained from this measurement is $\sim$0.02 ms. A complete analysis of the systematic errors is in progress.

Measurement of the non-analogue $0^+ \rightarrow 0^+$ transition in ^{38m}K

The determination of the transition strengths for non-analogue $0^+ \rightarrow 0^+$ decays provides a critical test of the model predictions for superallowed β decays. In particular, they provide a direct measurement of the isospin-mixing component of the Coulomb correction. Recently, I.S. Towner and J.C. Hardy [*ibid*] have recalculated the nucleus-dependent corrections for the nine well-known superallowed β emitters for several shell model effective interactions. The values of the square of the Fermi matrix element (δ_{C1}^1) to the first excited 0^+ state in ^{38m}K range from 0.062 to 0.186%. The only previous measurement obtained a limit of <0.28% [E. Hagberg *et al.*, Phys. Rev. Lett **73** 396 (1994)].

An experiment designed to measure this weak decay branch was carried out in October 2002. The fast tape transport system was used to collect and move the ^{38m}K samples out of the vacuum chamber and position them between two thin plastic scintillator paddles

each backed by a Compton suppressed (∼25%)HPGe detector from the 8π spectrometer. Details of this measurement were reported previously [see TRIUMF 2003 Annual Report for details].

This experiment was repeated in March 2006 using the full 8π spectrometer and SCEPTAR which increased the β-γ coincidence efficiency by a factor of 10 and substantially improved Compton suppression since the HPGe detectors were a factor of two further away from the source. The limiting factor in this measurement is the detection of a weak 1209 keV γ ray following the β decay of ^{38m}K ($t_{1/2} = 0.925$ s) to the first excited 0_2^+ state in ^{38}Ar at 3377 keV, in the Compton tail of the 2168 keV γ ray (with a branching ratio of 99.8%) following the β-decay of the long-lived isobaric contaminant ^{38}K$_{gs}$ ($t_{1/2} = 7.64$ min). A high powered Ta production target operating at 70 μA was used since yield measurements have shown that the ratio of beam intensities for ^{38}K$_{gs}$/^{38m}K is ∼10:1 (to be compared with 100:1 for the TiC target used in the previous study).

The beam on/off cycle used for this measurement is shown in Fig. 2. This cycle was chosen to optimize the ratio of ^{38m}K to ^{38}K$_{gs}$ decays and also provide a means to accurately determine this ratio. Approximately 2×10^9 ^{38m}K decays were observed. It is estimated that this should be sufficient to reduce the experimental branching ratio limit by a factor of 2. A detailed analysis of these data is in progress.

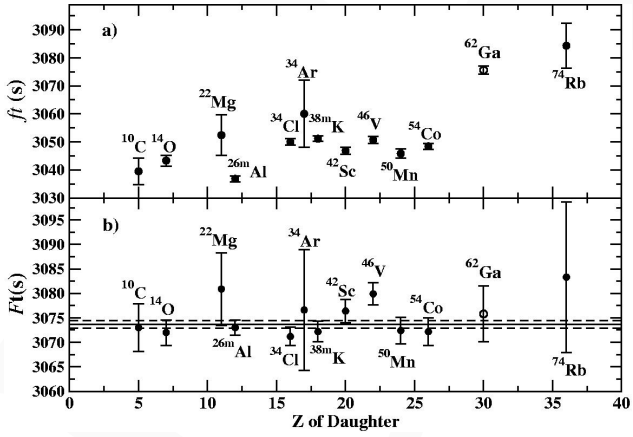

Fig. 1. The 13 precision superallowed (a) ft and (b) Ft values. The average Ft = 3073.66(75) s in (b) is obtained from the 12 values (solid circles) given in Table 1 of G. Savard *et al., ibid*, while the open circle for ^{62}Ga is from the present work.

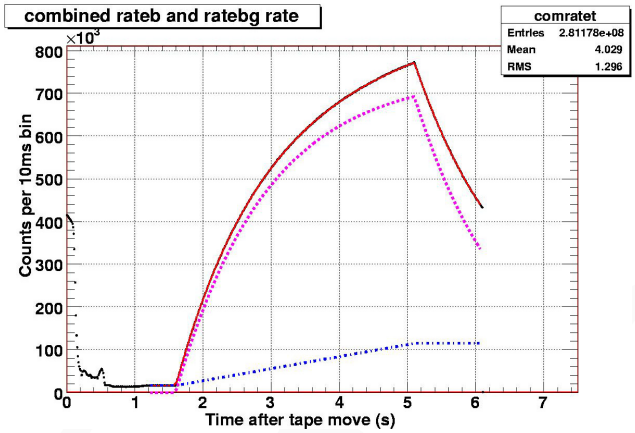

Fig. 2. A typical MCS spectrum obtained from the sum of all 20 elements of SCEPTAR. The tape was moved at the beginning of each cycle. After 1.6 seconds the radioactive ion beam was turned on for 3.5 s. After the beam was turned off the decay was followed for 1 s before repeating the cycle. The solid (red) line is a fit to the total buildup and decay curve using the known half-lives of ^{38m}K and ^{38}K$_{gs}$. The dotted (magenta) and dash-dot (blue) lines correspond to the individual ^{38m}K and ^{38}K$_{gs}$ decay components, respectively.

Experiment 909
Isospin symmetry breaking in superallowed Fermi β-decays

(G.F. Grinyer, Guelph)

Precision measurements of the ft values for superallowed $0^+ \rightarrow 0^+$ Fermi β-decays between isobaric analogue states provide demanding tests of the standard Model description of electroweak interactions. To date, superallowed ft values have been determined at the ±0.1% level for ten nuclei between ^{10}C and ^{62}Ga. Once corrected for small radiative and isospin symmetry-breaking effects, their consistency has confirmed the conserved vector current (CVC) hypothesis at the level of 3×10^{-4}. From these studies, the Cabibbo-Kobayashi-Maskawa (CKM) matrix element, V_{ud}, can be derived by comparing the β-decay data to pure leptonic muon decay. A recent improvement to the transition-independent radiative correction has improved the precision of V_{ud} by nearly a factor of 2. The most recent corrections applied to the superallowed ft values yield $V_{ud} = 0.97377(11)(15)(19)$, where the uncertainties are due to i) the experimental ft values combined with transition-dependent radiative corrections, ii) a discrepancy between two independent calculations of the isospin symmetry breaking corrections, and iii) the remaining uncertainty associated with the transition-independent radiative correction which is expected to be improved upon further [Marciano and Sirlin, Phys. Rev. Lett. **96**, 032002 (2006)]. The precision of V_{ud} may therefore ultimately be limited by the discrepancy in the nuclear-structure depen-

dent corrections δ_C which account for the breaking of perfect isospin symmetry by charge dependent forces in the nucleus.

Experiment 909 involves a series of measurements with the 8π γ-ray spectrometer and the scintillating electron positron tagging array (SCEPTAR) aimed at constraining the abovementioned isospin symmetry-breaking corrections in superallowed Fermi β-decays. This program will take advantage of the unique radioactive ion beams available at ISAC to study decays in which the predicted δ_C corrections show the greatest model sensitivity. An initial focus of Expt. 909 will be on half-life and branching ratio measurements for ^{34}Ar, with the aim of establishing the superallowed ft value at the $\pm 0.1\%$ level. These measurements will be carried out by collecting samples of ^{34}Ar at the centre of the 8π and following their decay for $\sim$30 halflives by time-stamping γ-rays emitted from excited states in the daughter, ^{34}Cl, populated in Gamow-Teller decay branches of ^{34}Ar.

Tests of the experimental techniques to be employed in Expt. 909 were carried out with radioactive ^{26}Na beams. This isotope was chosen because: i) high yields were available from existing ISAC surface ion sources, ii) the half-life ($\sim$1.07 s) is similar to that of ^{34}Ar ($\sim$0.84 s), iii) the daughter ^{26}Mg is stable, and iv) $\sim$99% of ^{26}Na β-decays are followed by an 1809 keV γ-ray transition in ^{26}Mg, facilitating tests of the γ-ray counting half-life technique to be employed for ^{34}Ar. To this end, a beam of $\sim 10^6$ ^{26}Na ions/s was delivered to the 8π spectrometer in April 2004. A sample decay curve obtained from a gate on the 1809 keV γ-ray in ^{26}Mg is presented in Fig. 1. Before the half-life of ^{26}Na can be reliably extracted from these data and compared to the high precision result obtained previously at ISAC, $T_{1/2} = 1.07128 \pm 0.00025$ s [G.F. Grinyer *et al.* Phys. Rev. C **71** 044309 (2005)], it is necessary to quantify all rate dependent systematic effects such as detector pulse pile-up. While pulse pile-up has been qualitatively understood for decades, these effects have not been understood quantitatively to the level of 0.05% necessary for superallowed half-life measurements. A detailed study of detector pulse pile-up via a Monte Carlo simulation combined with the relatively high-rate beam of ^{26}Na at ISAC has, for the first time, allowed a quantitative understanding of detector pile-up to the required level of precision. In our experiment, which aimed to test the methodology, we purposely increased the probability of pile-up, and hence the size of the corrections to be applied to the raw data, by inserting ^{56}Co sources into the 8π array and increasing the amplifier shaping times to the unusually large value of 6 μs. Following a correction of nearly 30 σ for these effects, the half-life of ^{26}Na was determined via γ-ray photopeak counting to a precision of $\sim$0.06% and is in excellent agreement with the previous result obtained at ISAC [G.F. Grinyer *et al.* Nucl. Instrum. Methods Phys. Res. A, submitted (2007)].

As a first test of the new ISAC FEBIAD ion source, 48 hours of ^{34}Ar beam was delivered to the 8π spectrometer over 3 separate commissioning runs during a 3 week period in November and December, 2006. A γ-ray singles spectrum collected over 10 hours is presented in Fig. 2, with the most intense transition in the daughter ^{34}Cl at 666 keV indicated. Contaminant γ-ray peaks following the decay of ^{34m}Cl ($T_{1/2} = 32$ min) were also present in the beam. A sample decay curve obtained from a gate on the 666 keV γ-ray is presented in Fig. 3 (lower panel). This gate is, however, not purely the decay of ^{34}Ar as a small contamination due to bremsstrahlung radiation from high-energy ^{34}Cl β particles was also present. This is shown in Fig. 3, where a gate on what appears to be the background below the 666 keV γ-ray (Fig. 3, upper right panel – Gate (a)) reveals a time dependence with a half-life consistent with that of ^{34}Cl (Fig. 3, upper left panel). Following a gate on the 666 keV transition itself (Fig. 3, upper right panel – Gate (b)) the half-life of ^{34}Ar was then extracted using a two-exponential fit with the half-life of ^{34}Cl fixed at its known value, $T_{1/2} = 1.527$ s. Further refinements are being investigated such as removal of the bremsstrahlung radiation by examining β-γ coincidences in the 8π spectrometer and SCEPTAR.

A measurement of the half-life of ^{34}Ar through the β activity was explored through the use of SCEPTAR, however, the ^{34}Cl present in the beam and produced by the decay of ^{34}Ar was the dominant signal in the β counters as seen in Fig. 4 for a single run where the ratio of ^{34}Cl to the total activity was $\sim$70% when the beam is turned off. The large ratio of ^{34}Cl to ^{34}Ar, combined with the fact that the half-lives of parent and daughter differ by a factor of only 1.8 makes a measurement of the ^{34}Ar half-life through the β activity extremely difficult to achieve at the required level of 0.05%.

From these results it is clear that the amount of Cl (both ^{34m}Cl and ^{34}Cl) present in the beam must be reduced in order to achieve a measurement of the half-life of ^{34}Ar to 0.05%. The first test of the FEBIAD ion source has produced encouraging results and improvements are envisioned that will increase the yield of ^{34}Ar to sufficient intensity ($>10^5$ s^{-1}). An improved ^{34}Ar beam is anticipated to be delivered to the 8π spectrometer in the fall, 2007.

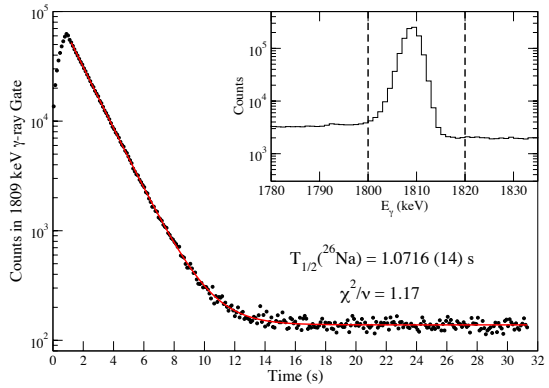

Fig. 1. Typical growth and decay curve of ^{26}Na obtained with the 8π spectrometer from a γ gate on the 1809 keV photopeak events in the γ-ray singles spectrum (inset).

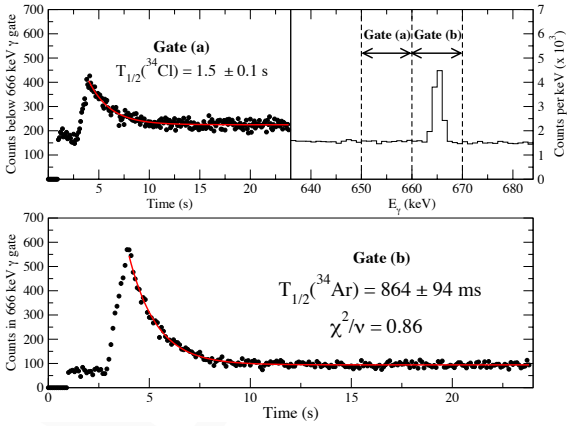

Fig. 3. (Upper left) Growth and decay curve from ^{34}Cl bremsstrahlung radiation obtained from a gate (Gate (a) – upper right) on the background just below the 666 keV transition. Following a gate on the 666 keV transition itself (Gate (b)) the growth and decay curve of ^{34}Ar is obtained but is also contaminated by ^{34}Cl bremsstrahlung which can be accounted for in the fitting procedure.

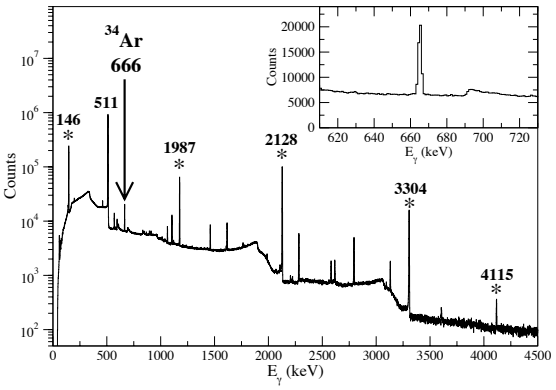

Fig. 2. Sum γ-ray singles spectrum obtained with the 8π spectrometer comprising 10 hours of $A = 34$ beam with γ-rays from a contamination of ^{34m}Cl indicated by (*). Inset: The 666 keV γ-ray in the daughter ^{34}Cl that follows the decay of ^{34}Ar.

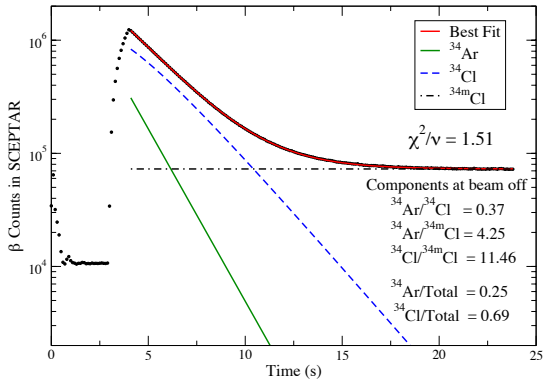

Fig. 4. Typical growth and decay curve obtained from the sum of all 20 SCEPTAR plastic scintillators for a single run. The contributions of ^{34}Ar, ^{34g}Cl, and ^{34m}Cl to the composite curve demonstrate that ^{34}Ar is only a small component of the total β activity.

Experiment 956

Search for tensor interactions in recoil nucleus singles in decay of polarized ^{80}Rb

(J.A. Behr, TRIUMF; J.R.A. Pitcairn, UBC)

Progress in tensor interaction search

Scientific motivation The recoiling daughter nuclei from the β decay of polarized nuclei have spin asymmetry $A_{\rm recoil} \approx 5/8\ (A_\beta + B_\nu)$ [Treiman, Phys. Rev. **110**, 448 (1958)]. This vanishes in the allowed approximation for pure Gamow-Teller decays, making it a very

attractive experimental observable because knowledge of the nuclear polarization at 10% level is sufficient to be competitive.

Analysis of the data taken in December, 2005 proceeds. We have completed the determination of the nuclear polarization from the atomic fluorescence diagnostic, which was the basis for the M.Sc. thesis of D. Roberge. We have understood most of the backgrounds and most of the modelling is completed.

Higher-order corrections "Recoil-order" corrections produce a nonzero $A_{\rm recoil}$ within the standard model. We estimate $A_{\rm recoil}$ to be $\sim$–0.03 by using $b = 4.7$ A c, where A is the atomic number and c the Gamow-Teller matrix element. (This ignores a matrix element of orbital angular momentum contributing to b, and the d term entirely.) A postdoc in the Theory group, J. Holt, has expertise in shell models in this mass region with magnetic multiple transitions that have similar operators.

Tensor interaction developments The PIBETA collaboration had reported a statistically significant deviation from the standard model [Frlež, Phys. Rev. Lett. **93**, 181804 (2004)] in $\pi \to \nu e \gamma$ decay that could be explained by a finite tensor interaction. But further data-taking dedicated to the task has produced a result with higher precision that is consistent with no tensor interaction [Pocanic, DNP (2006)]. These limits and those from TWIST appear to be on tensor interactions coupling to left-handed νs.

Experimental geometry

The Eept. 956 geometry is shown in Fig. 1. The detection system for ^{80}Kr recoils is similar to that in Expt. 715. A uniform electric field collects ions produced in β decay to a microchannel plate (MCP) Z-stack for time readout, backed by a position-sensitive resistive anode. A second MCP detector on the opposite side was added to detect low-energy atomic shakeoff electrons. The positive ions produced in β^+ decay will produce at least one electron, so this technique increases the efficiency for recoil detection by a factor of about 50 compared to β^+ detection (which had solid angle 1% in the Expt. 715 geometry).

Understanding of time-of-flight (TOF) spectrum We show a typical TOF spectrum in Fig. 2, deconstructed into its components. The different charge states are separated in TOF by a uniform 0.8 kV/cm electric field. Charge states 1 and 2 are relatively clean of background. Ions from the 1.4% electron capture branch have a large spin asymmetry and contaminate the higher charge states. Note that only about 15% of the β^+ decay produces positive ions, as opposed to most of the electron capture decays.

We measured the background from β^+s striking the electron detector by lowering the bias voltage of the detector to exclude the atomic electrons. That background mostly has the expected large spin asymmetry governed by the ν asymmetry. There is in addition a 1% background around 1.2 μs that shows a very small asymmetry and a definite localization on the lower part of the ion MCP. This background also appears in natural backgrounds and γ-ray source measurements, and may be due to an electronic artifact. Although its origin is not fully understood, we have measured it via this technique to sufficient accuracy.

Progress in polarization determination

As we described last year, to successfully keep the atoms from expanding during the optical pumping process, we left the MOT quadrupole magnetic field on at all times, with a 2.5 G uniform bias magnetic field along the optical pumping axis. Then we could quickly alternate MOT light and optical pumping light on a 60 μs duty cycle.

The polarization was measured by the time dependence of the atomic excited state population during the optical pumping, monitored by non-resonant photoionization with a small pulsed laser. The M.Sc. thesis of D. Roberge was completed, and the result was a vector polarization of 0.87 ± 0.05. A notable advance was full modelling of the optical pumping process in the presence of a transverse magnetic field. The atomic measurement is difficult to interpret with the MOT quadrupole field left on, because the varying Zeeman shifts produce different amounts of fluorescence from different positions within the trapped cloud.

Further atomic diagnostics measured the polarization of the fluorescence from ^{41}K atoms in the same geometry. These were in reasonable agreement with the measurements of the excited-state population.

The polarization was independently measured by the β^+ asymmetry using plastic/CaF_2(Eu) phoswich detectors, in coincidence with shakeoff electrons to minimize sensitivity to decays from untrapped atoms. The phoswiches are located at –30° and 150° with respect to the polarization direction, out of the plane of Fig. 1. Including the β energy spectrum properly in the modelling showed that a naive average over the asymmetry of the two main final states (which have asymmetry 1 and –1/2) was very misleading. Including the energy dependence of the states shows a polarization of 0.48 ± 0.04. Since it is still possible there are unknown backgrounds here, the true answer should lie somewhere in between this and the atomic polarization diagnostics.

Thus the nuclear vector polarization achieved is 0.68 ± 0.20. This is adequate because the present observable vanishes, though the sensitivity to $A_{\rm recoil}$ does

scale with the polarization. In retrospect it would have been wiser to turn the B field on and off and try to minimize the cloud expansion by making the atoms colder.

Other work We have also further developed the 405 nm laser for use for polarization probing. A simple cover for the laser has decoupled it from local temperature oscillations and greatly improved its long-term stability. We can pulse the 405 nm laser in coincidence with the 532 nm photoionizing laser to avoid perturbing the polarization. We used these improvements to measure the ^{39,41}K $5P_{1/2}$ isotope shift and submitted it for publication. When ^{37}K polarization development resumes, this laser should be very helpful to probe the hyperfine population of the ground state atoms.

Summary and future

Figure 3 shows a projected exclusion plot for tensor interactions, assuming Expt. 956 achieves its 0.007 statistical error and that its result is in full agreement with the standard model. It would then be complementary to other tensor interaction searches in β decay with similar errors. Whether to pursue the experiment any further would depend strongly on the size of the recoil order corrections from theory and the uncertainties in the shell model calculation. Measurement of the complementary case ^{82}Rb could also be contemplated.

The $LaBr_3$ detector that LADD is developing (that may be available for Expt. 1127) would allow a much better determination of the asymmetry to decays to the excited 2^+ state, as it would have sufficient energy resolution and be free of the count rate problems of the germanium detector.

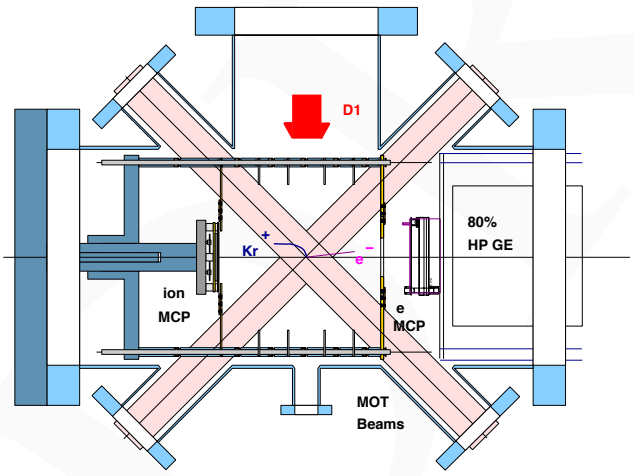

Fig. 1. TRINAT apparatus. The MCP for ion detection has position-sensitive resistive anode readout. An MCP for electron detection and HPGe detector are added for ^{80}Rb decay asymmetry. The ^{80}Rb is spin-polarized by optical pumping with D1 light from a 50 mW diode laser.

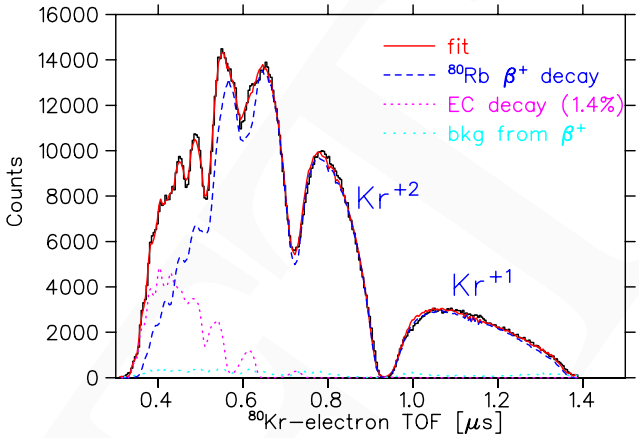

Fig. 2. Time-of-flight (TOF) spectra for recoil coincidences with shakeoff atomic electrons, showing decomposition into β^+ decay and backgrounds. The small electron capture branch produces large corrections for the higher charge states, and is modelled here assuming charge state distributions from X-ray photoionization [Carlson, Phys. Rev. **151**, 41 (1966)]. A 3% background from β^+s striking the electron detector is determined by biasing the detector to exclude low-energy electrons.

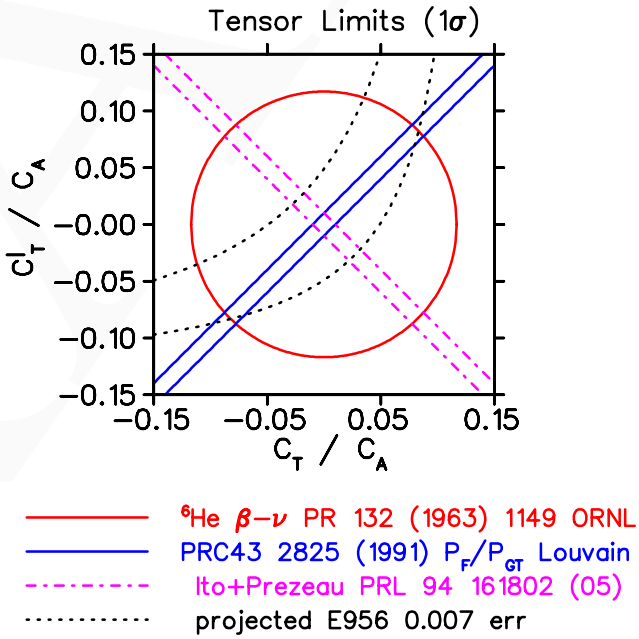

Fig. 3. Exclusion plot showing potential complementarity of Expt. 956 potential constraints, assuming a statistically dominated 0.007 asymmetry error and agreement with the standard model.

Experiment 964
TATIC – TRIUMF annular chamber for tracking and identification of charged particles

(G. Ruprecht, TRIUMF)

Introduction

The basic functionality of TACTIC is described in previous Annual Reports. In short, TACTIC is a time

projection chamber for ion tracking. The cylindrical design makes it possible to separate the target from the detection region and hence apply higher beam currents. Since TACTIC also covers a large solid angle, very low cross sections can be measured. The cylindrical design is only feasible using a gas electron multiplier (GEM) foil which has now been thoroughly tested in a planar mock chamber.

Garfield

Garfield is a simulation package which allows us to simulate the drifting of electrons through TACTIC in 2 and 3 dimensions. Garfield also calculates key drift parameters of the detector gas, such as the electron drift velocity, longitudinal and lateral diffusion, Townsend coefficients and attachment coefficients. This allows us to calculate drift times, position resolution and ultimately simulate the signals we can expect to measure with TACTIC.

Thus far Garfield has been used as an aid to design the concentric cathode cage for TACTIC. The cathode cage is designed to trap ionization electrons created by the beam as it is attenuated in the chamber. The separation, thickness and potential of the wires has been adjusted to trap the maximum number of electrons (see Fig. 1). Almost all electrons created inside the radius of the inner cathode drift onto that electrode. Only electrons created between the two sets of wires manage to escape into the drift region at $r > 1.2$ cm.

Electron diffusion in the detection and induction regions of TACTIC is an important factor in both energy and position resolution. Garfield has been used to estimate the diffusion in both regions. Diffusion increases with the square root of distance travelled by the electrons, so the diffusion in the drift region dominates over the contribution from the induction region. Garfield calculations show that the longitudinal electron diffusion corresponds to a difference in drift velocities of about 2% of the total drift time. The lateral diffusion over the drift region corresponds to about 1 mm. These values can be calculated from the diffusion coefficents in Fig. 2.

Geant4

Two main problems make Geant4 difficult to use for ion physics. Firstly, there exists no process for single Coulomb scattering, and secondly, there are unacceptable deviations of the stopping powers and ranges of ions as compared to the values given by SRIM 2003. The first problem was solved by implementing our own Coulomb scattering process that has been described in the 2005 Annual Report. The second problem and its solution are described in the following.

Geant offers several models for low-energy stopping powers. They are all based on tables of coefficients for protons in different materials but with slightly different formulas and coefficients; stopping powers for heavier ions are scaled from the proton stopping powers using the effective charge model. As it turned out, even the latest models are quite out-of-date. Although there are small deviations between them, they all are based on Ziegler's SRIM/TRIM coefficients from 1985 that in turn are based on an evaulation of all experimental data. However, SRIM 2003 which is generally accepted as the reference for stopping powers is based on a complete new evaulation of experimental data and there are some considerable changes in them. Unfortunately, undocumented slight changes have been made in the fit formulas and the new coefficients can not be used to just replace the old ones in Geant4. To overcome this dilemma, we extracted the stopping-power curves from SRIM 2003 and fitted an extended formula to these data. As a result, the new modified energy loss process exactly matches the SRIM 2003 data. An evaluation of this energy loss process, in combination with elastic scattering for all ions in all materials, is still ongoing.

Test chamber measurements

Prototypes of the flash ADC VME modules "VF48" devoloped at the University of Montreal have finally been delivered and we can present here some first results of particle tracking in the planar mock chamber. We employed a TRIUMF-made 32-channel amplifier board provided by Leonid Kurchaninov as used for the LiXe project for the amplification of the GEM signals.

Figure 3 shows some ion trajectories in the mock chamber filled with 90% He/10% CO_2 gas mixture at atmospheric pressure. The trajectories can be visualized on-line with a new analyzer implemented in collboration with Jonty Pearson. The analyzer can remotely connect with the MIDAS DAQ system and visualize the events with a high frame rate. Additional (slowly changing) histograms are provided on a Roody port. The rate was limited by the still missing interrupt feature of the VF48 module. This will be provided with the next firmware update.

The largest problem is the selection of "good" events. The range of the 3.1 MeV α particles from the source in this gas mixture is about 5 cm but the height of the drift frame is only 2 cm. Therefore many ions hit the wall and produce incomplete signals. This can be clearly seen from Fig. 5 where the total energy is drawn versus the slope of the trajectory. If the ions hit the wall no further drift electrons are produced and the collected charge is incomplete, leading to a wide energy spread (the source is not quite centered, hence the asymmetry). Therefore, only a small region around slope = 0 can be used for an energy measurement. The gas is also slightly contaminated so that some drift elec-

trons are absorbed when moving towards the GEM, further reducing the resolution. For the next series of tests we will have an improved test chamber with a better sealing, a larger volume and a higher number of sensitive strips.

Construction

The initial concept drawings for the TACTIC detector were made at TRIUMF. These drawings formed the basis for the technical designs provided by the Design Workshop at the CCLRC Daresbury Laboratory, UK. Over several meetings between the University of York and the Daresbury Design Group, the designs were finalized. In May Pierre Amaudruz who had drawn up the initial concept of TACTIC met with the York and Daresbury groups to confirm the finalized design and the Daresbury group provided the University of York with a set of working technical drawings.

In summer construction of the TACTIC chamber commenced in the Mechanical and Electronic Workshops at the Department of Physics, University of York, UK. Figure 6 shows the interior of the detector support structure together with the end flanges. The beam pipe which will conjoin with the support structure being built at TRIUMF is clearly visible. The construction of the support structure for the GEM and anode (the white plastic cylindrical assembly visible in Figs. 6 and 7) was particularly challenging but has now been completed.

The design of the cathode was arrived at following Garfield simulations of possible arrangements of wires that might contain the ionization in the gas caused by the beam passing through it. Final construction of this unique cathode structure is under way.

Other aspects of the construction are being undertaken at TRIUMF. A gas handling system capable of accurately regulating the pressure of the gas flowing through the detector is currently being built. The support structure which will mount the TACTIC detector onto the beam line at ISAC is also being designed and built by the TRIUMF group.

Test assembly of the TACTIC detector is about to commence at the University of York. Once this has established a working procedure for construction of the detector, the full detector (including the GEM) will be built in a clean room environment. Benchtop tests will establish the vacuum integrity of the detector and, using suitable radioactive sources, physical signals will be extracted from the detector. These tests will be undertaken with the participation of some members of the TACTIC collaboration from TRIUMF. It is envisaged all tests at York will be completed by the end of April, 2007 and the detector will then be transported to TRIUMF in preparation for in-beam tests in summer, 2007.

Schedule

A beam request (Expt. 964, Beam Request ID 581) has been submitted for early summer, 2007 for ^{11}B beam and, if there is sufficient time, for ^{10}B and ^{7}Li also. Elastically scattered ^{11}B will provide a full test of TACTIC in preparation for the running of Experiment E964 (^{8}Li(α,n)^{11}B) by actually detecting the recoil ion at similar energies to that expected in the final experiment.

The full schedule of tests to be undergone in the stable beam run is to be finalized but will include:

1. Confirmation of the optimum gas mixture to be used (previously studied using a planar test chamber at TRIUMF – see 2005 Annual Report 2005, Expt. 964).
2. Test of the capabilities of the VF48 DAQ system (data will also be collected with a conventional DAQ for off-line comparison).
3. Study of the particle identification capabilities of the detector by studying the differences between the signals detected from scattered ^{11}B, ^{10}B and ^{7}Li.

It is expected that the analysis of these test data will confirm the readiness of TACTIC for taking ^{8}Li beam for Expt. 964 in late 2007.

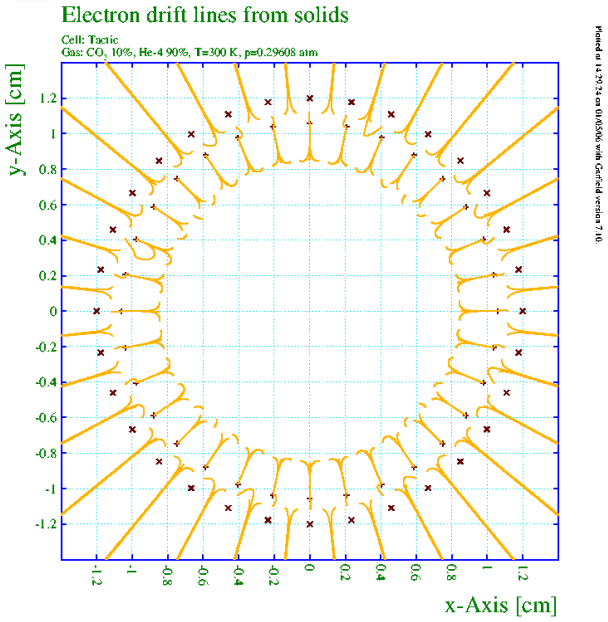

Fig. 1. A Garfield simulation of the TACTIC cathode. The black crosses represent the concentric arrangement of wires; there are 32 in each ring. The inner wires are held at a potential of –1800 V, the outer wires at –2000 V.

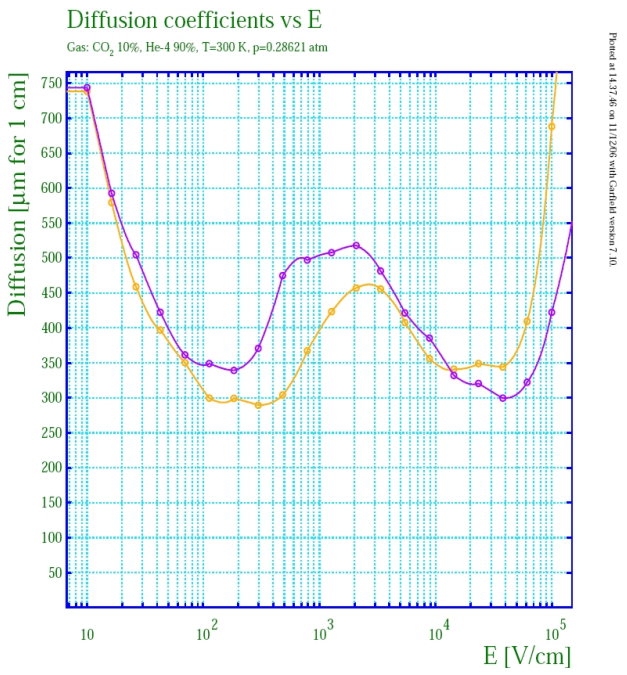

Fig. 2. Longitudinal (yellow) and lateral (purple) diffusion coefficients for a 90% He, 10% CO_2 gas mixture at 290 mb and 300 K.

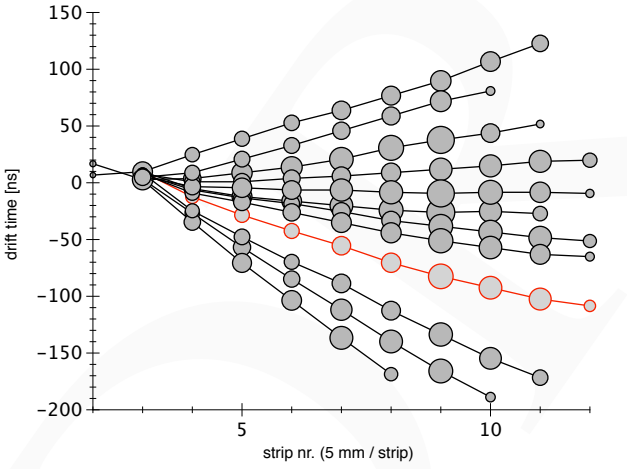

Fig. 3. Drift time vs. strip number for some selected events. The 3.1 MeV α source is placed in the middle of a planar drift chamber above strip number 3. Since the drift time is assumed to be proportional to the distance to the GEM, we obtain a projected picture of the ion trajectory. There is no trigger for the emission of the α's, so the trajectories have been normalized to $t = 0$ at strip number 3. The size of the blobs represents the height of the signal, assumed to be proportional to the energy loss per strip.

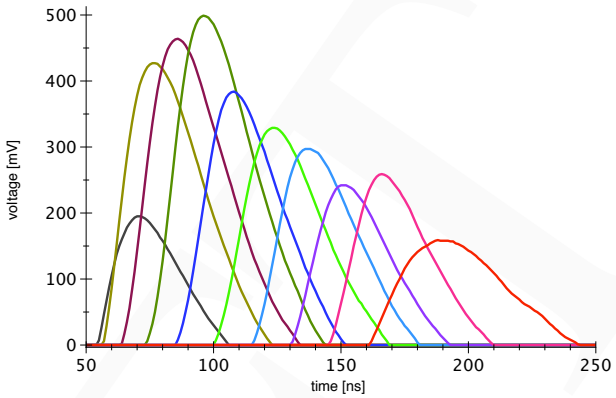

Fig. 4. Signals from the event highlighted in the previous figure. The Bragg peak can clearly be seen.

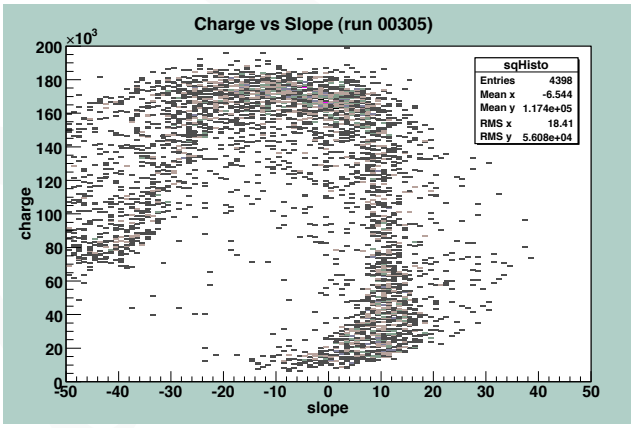

Fig. 5. Integrated charge (arbitrary units) vs. slope. The slope is the mean time difference (in ns) per strip of an ion track. Positive slope means that the ion moves towards the cathode.

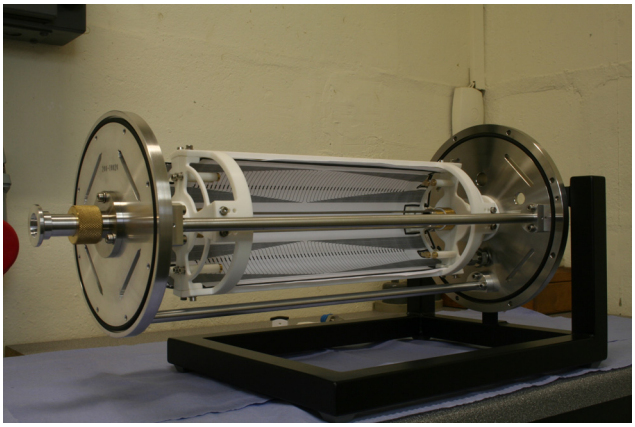

Fig. 6. The TACTIC prototype in York – total view.

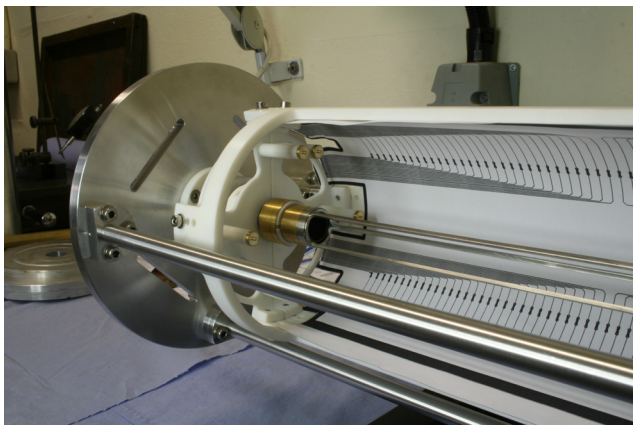

Fig. 7. The TACTIC prototype in York – beam inlet.

Experiment 973
Study of coexisting collective phases far from stability: systematic decay spectroscopy of the $N = 90$ isotones
(W.D. Kulp, J.L. Wood, Georgia Tech)

Introduction

The rapid change in nuclear shape from a near-spherical to a well-deformed shape as neutron number increases near stability at $N = 90$ is one of the greatest challenges to collective nuclear models. These nuclei exhibit a variety of coexisting collective structures, the nature of which has been the subject of inquiry for nearly five decades. Experiment E973 is a systematic study of the doubly-even $N = 90$ isotones ^{146}Ba, ^{148}Ce, ^{150}Nd, ^{156}Dy, ^{158}Er, and ^{160}Yb, through the radioactive decay of the parent isotopes ^{146}Cs, ^{148}La, ^{150}Pr, ^{152}Pm, ^{156}Ho, ^{158}Tm, and ^{160}Lu (on-line) and ^{152,154}Eu (off-line) using the 8π spectrometer together with the moving tape collector, PACES, DANTE, and SCEPTAR.

Very detailed spectroscopic information has been acquired [Kulp, *et al.*, Phys. Rev. Lett. **91**, 102501 (2003); *ibid.*, Phys. Rev. **C69**, 064309 (2004); *ibid.*, Phys. Rev. **C71**, 41303 (2005); *ibid.*, Phys. Rev. **C73**, 014308 (2006)] for ^{152}Sm and ^{154}Gd using the 8π spectrometer when it was at the Lawrence Berkeley National Laboratory 88-Inch Cyclotron Facility. As part of the Expt. 973 experimental program, the reconfigured 8π spectrometer has been used at TRIUMF/ISAC-I to study ^{156}Dy, ^{158}Er, and ^{160}Yb.

Data were acquired in 2004 on the excited structure of ^{156}Dy through the decay of three isomers of ^{156}Ho, and additional data on the long-lived ^{156g}Ho isomer were collected in 2006. Data on ^{158}Er were acquired through the decay of two isomers of ^{158}Tm in 2005. In 2006, data were acquired on the structure of ^{160}Yb from the decay of two isomers of ^{160}Lu. Analysis of all data sets is presently under way: the $A = 156$ decay chain is part of the Ph.D. thesis work of Serkan Dursun; the $A = 158$ decay chain is part of the Ph.D. thesis work of Nathaniel Brown; and the $A = 160$ decay chain is being used to train undergraduate students at both Georgia Tech and the University of Guelph.

Evidence of shape coexistence at $N = 90$

Analysis of conversion-electron spectra from PACES and γ-ray spectra from the 8π reveals new electric monopole ($E0$) transitions in ^{156}Dy and ^{158}Er. The $E0$ transitions are between the $J^\pi = 2^+$ and 3^+ states of the excited $K^\pi = 2^+$ bands in these two nuclei, as shown in Fig. 1. The corresponding structures in the isotone ^{154}Gd have known $E0$ transitions between the 2^+ and 3^+ states, indicating a systematic feature of the $N = 90$ nuclei.

Crucial for the understanding of the $N = 90$ transition region, the $E0$ transitions are evidence of coexisting shapes and mixing in this region. Complementary studies of ^{152}Sm through multiple-step Coulomb excitation and inelastic neutron scattering reveal a strong $E2$ transition from the 2^+ state of the second excited $K^\pi = 2^+$ band to the 2^+ state of the second excited $K^\pi = 0^+$ band. This transition, with a $B(E2)$ value of 26 W.u., suggests that the second $K^\pi = 2^+$ band is an analogue of the γ excitation of the ground state, i.e., it is a collective excitation built upon the second $K^\pi = 0^+$ band.

A contributed talk [Kulp *et al.*, Bull. Am. Phys. Soc. **51**, 38 (2006)] was presented at the American Physics Society Division of Nuclear Physics annual meeting in Nashville, TN in 2006 describing the discovery of coexisting $K^\pi = 2^+$ bands in $N = 90$ nuclei using $E0$ transition signatures.

The decay of ^{160}Lu $\rightarrow$ ^{160}Yb

Beam time to study the excited structure of ^{160}Yb populated through the β decay of ^{160}Lu was allocated in July. The strongest γ-ray transition in ^{160}Yb, at an energy of 243.4 keV, is indicated in a portion of the projection of the γ–γ coincidence matrix as shown in Fig. 2. It is evident from this that ^{160}Lu was only a small component of the beam, yet transitions in ^{160}Yb are isolated using γ–γ coincidence spectroscopy. Two γ-ray spectra in coincidence with 243.0 and 244.5 keV γ-ray transitions are shown in Fig. 3. The 396 and 577 keV γ-ray transitions are the next two strongest transitions in the ^{160}Yb scheme, and comparison of the two spectra shows that these transitions are more prominent in the 243 keV gate. The known ^{160}Lu $\rightarrow$ ^{160}Yb decay scheme has been principally validated through γ–γ coincidences; further analysis of these data requires identification of weak transitions in the strong isobaric contaminants.

Comprehensive decay spectroscopy with the 8π and PACES

In Fig. 3, the γ-ray spectrum in coincidence with the 245 keV γ-ray shows a γ-ray at 400 keV, and we tentatively assign both of these new γ-rays to the decay scheme of ^{160}Tm. The basis for this assignment is evident in Fig. 4, where PACES spectra in coincidence with γ-rays detected in the 8π and conversion electrons detected in PACES are presented. The strong Tm X-rays in all of these spectra are evidence that these are all new transitions between excited states in ^{160}Tm. The 245 K- and L-conversion electron lines in coincidence with the 400 keV γ-ray are further evidence that these two transitions are in coincidence (cf. Fig. 3b), and the energy difference between the K- and L- lines is appropriate for the electron binding energies for Tm.

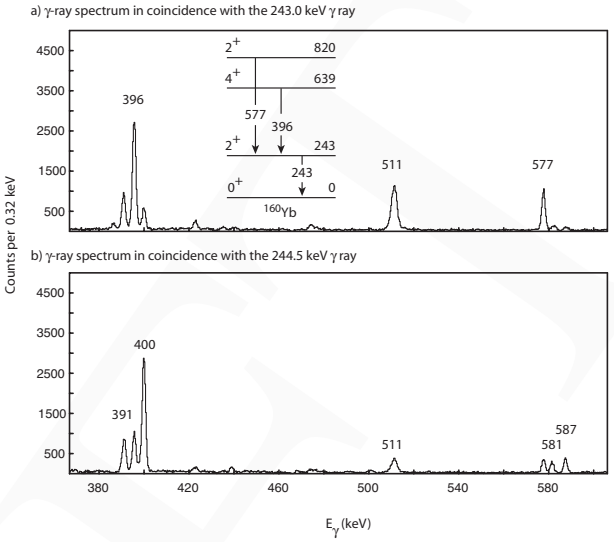

Fig. 3. Spectra showing γ-rays in coincidence with a) the 243 keV γ-ray in ^{160}Yb and b) the 245 keV transition in ^{160}Tm. The 396 and 577 keV transitions in ^{160}Yb are clearly accentuated in the 243 keV gate.

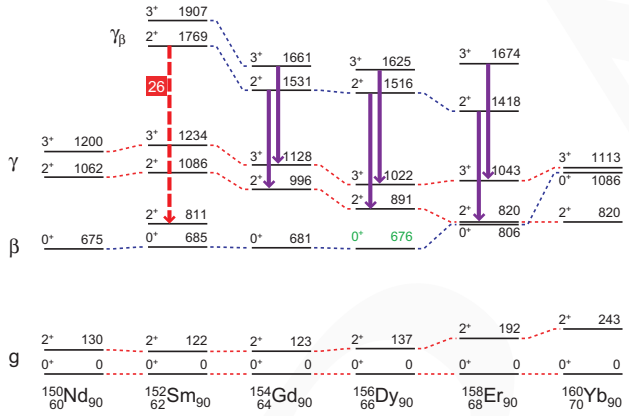

Fig. 1. Electric monopole ($E0$) transitions between the $J^\pi = 2^+$ and 3^+ states of excited $K^\pi = 2^+$ bands are indicative of mixing between two coexisting shapes in the $N = 90$ isotones.

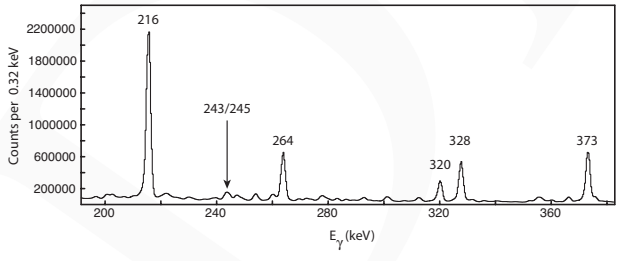

Fig. 2. Due to isobaric contaminants, the $2_1^+ \rightarrow 0_1^+$ 243.4 keV transition in ^{160}Yb is all but invisible in the projection of the γ–γ coincidence matrix.

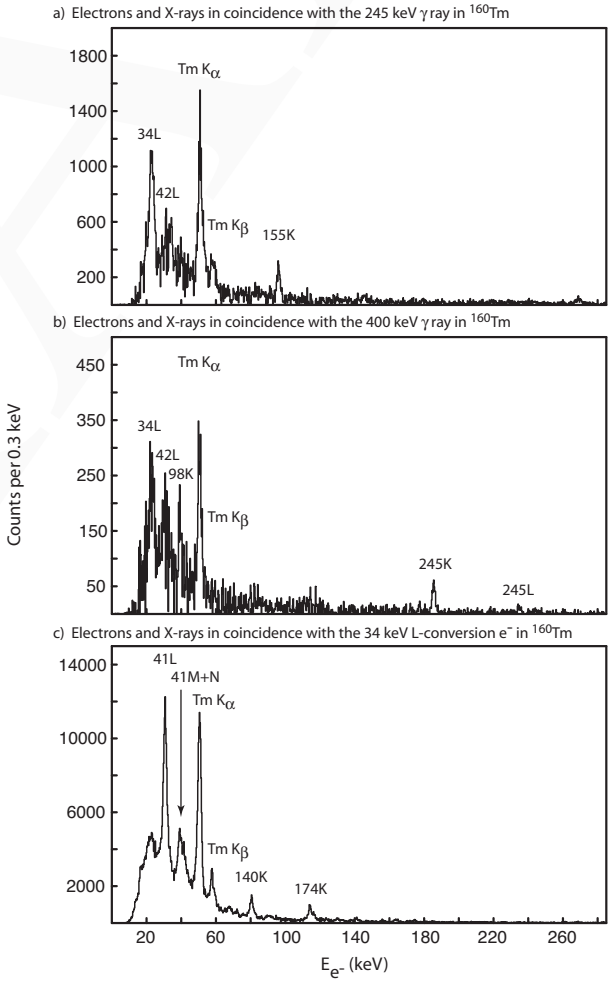

Fig. 4. Electron and X-ray spectra in coincidence with γ-ray and conversion-electron transitions in ^{160}Tm.

Experiment 983
Direct measurement of the astrophysical ^{11}C$(p,\gamma)^{12}$N reaction at DRAGON
(W.P. Liu, CIAE)

In December, 2003, the EEC approved the proposed measurement of the astrophysical reaction rate of ^{11}C$(p,\gamma)^{12}$N with 20 shifts. At the temperature of astrophysical relevance, the ^{11}C$(p,\gamma)^{12}$N reaction is believed to be dominated by the direct capture into the ground state and the resonant captures via the first (2^+) and second (2^-) excited states of ^{12}N. It was mentioned in this proposal that the measurement of the ^{11}C$(p,\gamma)^{12}$N reaction will focus on the second (2^-) resonance in the case of lower beam intensity or limited beam time. However, there has been some new experimental information on the ^{11}C$(p,\gamma)^{12}$N reaction since that time. Therefore, we have revised the experimental plan, and will focus on the measurement of the 2^+ resonance which dominates the ^{11}C$(p,\gamma)^{12}$N reaction above $T_9 = 0.35$ in the astrophysical sites of rap-II and rap-III linking the pp-chains and rp-process.

Introduction

Nuclear capture reactions, such as (p,γ) and (α,γ), play a crucial role in the evolution of stars. The ^{11}C$(p,\gamma)^{12}$N reaction may play an important role in the evolution of massive stars with very low metallicities, which is one of the key reactions of rap-II and rap-III. ^{11}C$(p,\gamma)^{12}$N is dominated by the 2^+ resonance at $T_9 > 0.35$ in the rap-II and rap-III chains.

In summary, although there are still large discrepancies for both direct capture and resonant capture contributions in the ^{11}C$(p,\gamma)^{12}$N reaction, the 2^+ state remains the most unsolved issue. Thus, the first experimental measurement of 2^+ resonance is crucial for determining the total rate of ^{11}C$(p,\gamma)^{12}$N and providing the most precise data to nuclear reaction network calculations.

Description of the experiment

For the narrow 2^+ resonance, the reaction rate can be parameterized as

$$N_A\langle\sigma v\rangle = N_A\Big(\frac{2\pi}{\mu kT}\Big)^{3/2}\hbar^2\omega\gamma\exp(-E_r/kT).$$

We will measure the thick target yield of the narrow 2^+ resonance in ^{11}C$(p,\gamma)^{12}$N. The maximum thick target yield can be related to resonant strength and resonance energy by

$$Y_{\max} = \frac{\lambda^2}{2}\frac{M_H + M_C}{M_H}\frac{1}{\varepsilon}\omega\gamma.$$

Thus, a direct measurement of the thick target yield at maximum would lead to the resonant strength and then resonant reaction rate.

In the experiment, the recoils will be detected using a DSSSD (double sided silicon strip detector), in coincidence with prompt γ-rays detected by BGO arrays. The reaction yield can be given by

$$Y = \frac{N_{\rm det}}{N_{\rm inc}\eta_{\rm tot}},$$

where $N_{\rm det}$ and $N_{\rm inc}$ are the total number of detected recoils and incident ions, respectively. The overall efficiency is

$$\eta_{\rm tot} = \eta_{\rm BGO}\cdot\eta_{\rm sep}\cdot\eta_{\rm char}\cdot\eta_{\rm DSSSD},$$

where $\eta_{\rm BGO}$, $\eta_{\rm sep}$ and $\eta_{\rm DSSSD}$ are the BGO array, transmission and DSSSD efficiencies, respectively, and $\eta_{\rm char}$ is the charge state fraction.

The reaction yields were then estimated around the resonance energy (E_r = 359 keV) based on the cross sections from indirect measurement, as shown in Fig. 1 and listed in Table I. Since Γ_γ of 2.59 meV is a theoretical calculation, only the uncertainty of Γ_p (0.91 ± 0.29 keV) was included in that of yields. In addition, the estimated yields were fitted as indicated by the solid line. We have also calculated the counting rates for coincidence of ^{12}N with γ-rays for specified experimental conditions, which are listed below:

- 1×10^8 ions/s ^{11}C beam intensity;
- 6 Torr hydrogen gas taget;
- 20% overall efficiency.

During the experiment, a gas-target pressure of 6 Torr can be maintained to within $\pm$1.6%. The overall efficiencies were extracted to be 21% and 30% for the previous ^{21}Na$(p,\gamma)^{22}$Mg and ^{26g}Al$(p,\gamma)^{27}$Si experiments, respectively. Thus, an overall efficiency of 20% was taken as a rough estimate in the present calculation. The coincidence rates are calculated in the case of 1×10^8 ions/s ^{11}C beam intensity, and listed in Table I. Based on the expected rates, about 50 events will be obtained for a certain beam energy at maximum yields if we spend 10 hours. The contamination of ^{11}B and ^{22}Na will be measured using 4 shifts of ^{11}B beam and 4 shifts of ^{22}Na. Therefore, the approved beam time of 20 shifts (240 hours) should be adequate for the measurement of a thick target yield curve with reasonable statistics. It should be noted that this estimate is rough due to the large uncertainty of available level parameters of 2^+ state in ^{12}N.

Conclusion

In conclusion, we updated the current status of the ^{11}C$(p,\gamma)^{12}$N reaction. We found that there is no experimental Γ_γ data for the 2^+ resonance contribution. The 2^+ resonance is important since it dominates the

^{11}C$(p,\gamma)^{12}$N reaction above $T_9 = 0.35$ in the astrophysical sites of rap-II and rap-III. We have estimated the reaction yields and counting rates for coincidence of ^{12}N with γ-rays and found that a direct measurement of 2^+ resonance in TRIUMF/DRAGON is feasible. As a result, this updated proposal will focus on the narrow 2^+ resonance measurement. The optimum beam intensity is greater than 10^8 pps. However, moderate beam intensities in the order of 10^7 pps is affordable. The required shift will remain at 20.

In December, we participated in a video conference organized by the EEC. The above modification of Expt. 983 was presented.

Table I. Expected reaction yields and counting rates of ^{12}N in coincidence with γ-rays.

$E_{\rm p}$ (keV)	$E_{\rm cm}$ (keV)	Yield	Rate (hr^{-1})
381.8	350	1.94×10^{-12}	0.1
387.3	355	2.87×10^{-12}	0.2
391.6	359	3.50×10^{-11}	2.5
392.7	360	6.03×10^{-11}	4.3
396.0	363	6.95×10^{-11}	5.0
401.5	368	6.89×10^{-11}	5.0
404.7	371	7.06×10^{-11}	5.1
409.1	375	2.31×10^{-11}	1.7
414.5	380	3.38×10^{-12}	0.2
420.0	385	2.81×10^{-12}	0.2

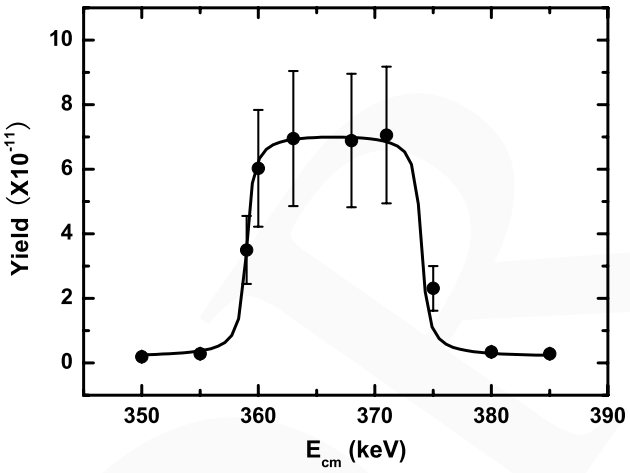

Fig. 1. Estimate of thick target yields of narrow 2^+ renonance of the ^{11}C$(p,\gamma)^{12}$N reaction around the resonance energy.

Experiment 992
Lifetime of the 4.03 MeV state in ^{19}Ne
(G. Ball, B. Davids, TRIUMF)

The ^{15}O$(\alpha,\gamma)^{19}$Ne reaction leads to the initial breakout from the hot CNO cycles that operate in Type I X-ray bursts, which are thermonuclear runaways on accreting neutron stars in binary star systems. Recent calculations have suggested that if the rate of this reaction were below a certain threshold, the periodic X-ray bursts observed from some accreting neutron stars would not occur. Hence the rate of this reaction is of considerable importance. However, direct measurements at the relevant energies would require (radioactive) ^{15}O beams of high intensity not presently available. Since the first theoretical investigation of this reaction, experimental data on the radiative and α widths of excited states in ^{19}Ne have been used to better constrain its rate. At temperatures below 0.6 GK the reaction rate is dominated by resonant capture to the first state above the α-emission threshold, lying at an excitation energy of 4.03 MeV.

The decay widths of the 4.03 MeV state in ^{19}Ne have until recently remained elusive. Its α width, Γ_α, has been experimentally unobservable on account of its small value. All published attempts to measure the α-decay branching ratio $B_\alpha \equiv \Gamma_\alpha/\Gamma$ have yielded only upper limits. Therefore the reduced α width of the analogue state at 3.91 MeV in ^{19}F has been used to estimate the α width. Early theoretical estimates of the reaction rate assumed the radiative widths of the ^{19}Ne and ^{19}F analogue states to be equal. Despite attempts to measure the lifetime of the state in ^{19}Ne itself that resulted in lower and upper limits, the analogue state has been the most reliable source of experimental information on the radiative width. With the recent report of the first measurement of the lifetime of the 4.03 MeV state, as well as more precise determinations of the excitation energies of this and other states in ^{19}Ne by a group at Notre Dame University, the experimental situation has improved dramatically. At TRIUMF we have carried out the second and third successful measurements of the lifetime of the 4.03 MeV state in ^{19}Ne, using a different reaction in which the recoil velocity was higher, allowing for a more precise lifetime determination.

Experiment 992 ran from September 5–12. The experiment was performed at the ISAC facility using the Doppler-shift attenuation method. A 34 MeV ^{20}Ne beam was incident on a 12.5 μm thick, ^{3}He-implanted Au foil target, populating the level of interest via the ^{3}He(^{20}Ne,α)^{19}Ne reaction. The ^{20}Ne beam and recoiling ^{19}Ne nuclei were stopped in the Au foil. The average beam intensity was 10 particle nA. De-excitation γ-rays were detected in coincidence with α particles using an 80% high-purity germanium (HPGe) coaxial detector placed at 0° with respect to the beam axis. The lifetime was determined from a lineshape analysis of this γ-ray energy spectrum. A second HPGe detector placed at 90° was shielded from the target by lead plates but recorded γ-rays from a weak ^{88}Y source. This second HPGe detector was used to monitor the

stability of the electronics. The detectors were located 9 cm from the target.

The scattering chamber was designed with a cold trap to ensure a clean target surface and also to prevent losses of the implanted ^{3}He. This was achieved using a narrow differential pumping aperture followed by a copper cylinder enclosing the path of the beam to the target. The copper cylinder was cooled using liquid nitrogen. To avoid any condensation of impurities on the surface of the target, the copper cylinder was not in direct contact with the target ladder. Indirect contact of the cold copper cylinder with the copper target ladder was achieved using BeCu fingers mounted on a boron nitride plate, which provided electrical isolation as well. This arrangement maintained a temperature difference between the copper cylinder and the target ladder. In this way the target was cooled below room temperature to ensure that ^{3}He did not diffuse out when heated by bombardment with a beam power of up to 0.3 W. Moreover, the colder surfaces surrounding the target foil and the beam path in front of it reduced the buildup of carbon and other contaminants on the target itself during the experiment.

The target foil was prepared at the Université de Montréal by implanting 30 keV ^{3}He ions into a 12.5 μm thick Au foil, yielding an areal ^{3}He number density of 6×10^{17} cm^{-2}. The implantation region was 0.1 μm thick. The foil was found to contain some surface deposits of carbon after the implantation process. The concentration of ^{3}He in the foil was monitored via yields of elastically scattered ^{3}He during the experiment. The beam was collimated to a 2 mm diameter spot on the target.

The α particles were identified by means of the energy loss (ΔE) and total energy (E) correlation using a silicon detector telescope. The telescope consisted of a 25 μm thick silicon detector for ΔE measurement and a 500 μm silicon detector for E measurement. Both the detectors were standard, circular, ORTEC transmission-type detectors with an active area of 150 mm^2. The detector telescope subtended a solid angle of 360 msr and was centred about the beam axis, allowing the detection of α particles with scattering angles less than 20°. A wide range of α particle energies arose from fusion-evaporation reactions with the carbon contaminant on the foil. The γ-ray energy spectrum obtained from the 0° HPGe detector in coincidence with α particles having the appropriate energies is shown in Fig. 1. The two peaks observed at 4.2 and 4.3 MeV are consistent with known ^{19}Ne transitions Doppler shifted appropriately for recoils moving with $v = 0.04\,c$. The data are presently being analyzed by UBC Ph.D. student Mythili Subramanian as part of her thesis work. It is anticipated that this will be the most precise measurement of the lifetime of the 4.03 MeV state yet.

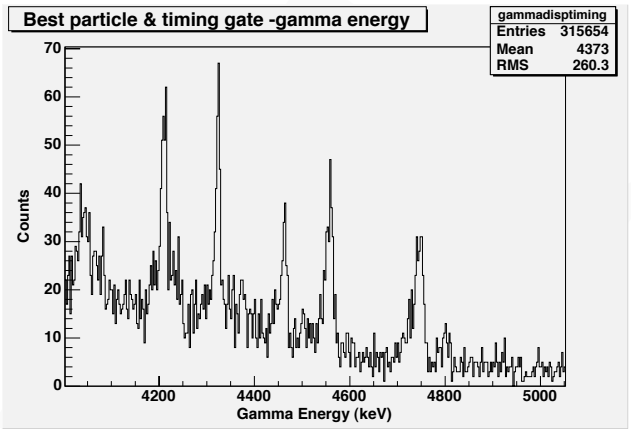

Fig. 1. Preliminary 0° Doppler-shifted γ-ray spectrum obtained in coincidence with α particles.

Experiment 1024
^{40}Ca(α,γ)^{44}Ti for astrophysics

(C. Vockenhuber, TRIUMF)

Introduction

^{44}Ti ($t_{1/2}$ = 58.9 ± 0.3 yr) is one of the few short-lived radionuclides which has been detected in space by γ-ray astronomy with COMPTEL [Iyudin *et al.*, Astron. Astrophys. **284**, L1 (1994)] and later with INTEGRAL [Renaud *et al.*, Astrophys. J. **647**, L41 (2006)] and thus confirms ongoing nucleosynthesis in our galaxy. Since it is conjectured to be produced predominantly in supernovae during the α-rich freeze-out, its measured abundance can be used to constrain supernova models. It has also been attempted to search for previously undiscovered young supernova remnants by γ-rays from the decay of ^{44}Ti; however, even with the improved sensitivity of INTEGRAL, only Cassiopeia-A showed a signal significantly above the background to date. This is in strong contrast with expectations from galactic supernova rates of a few SN per century, which indicates large uncertainties in our understanding of supernova explosions and/or the nuclear reactions relevant for ^{44}Ti production.

The ^{40}Ca(α,γ)^{44}Ti reaction plays a key role in ^{44}Ti production and was identified as one of the most critical reactions in network calculations [The *et al.*, Astrophys. J. **504**, 500 (1998)]. It has been studied partly in the past by non-inverse prompt γ-ray measurements [e.g. Cooperman *et al.*, Nucl. Phys. **A284**, 163 (1977)]. A recent integral measurement over a larger temperature regime by off-line counting of ^{44}Ti nuclei with accelerator mass spectrometry (AMS) showed a significantly larger ^{44}Ti yield compared to the prompt γ-ray data [Nassar *et al.*, Phys. Rev. Lett. **96**, 041102 (2006)]. The advantage of our measurement at DRAGON is

that we directly detect ^{44}Ti recoils and prompt γ-rays, which allows a detailed study of this reaction over a large energy range with sufficient resolution to resolve individual resonances.

In 2006 we completed the experiment with a three-week beam time of ^{40}Ca to cover the lower energies of the anticipated excitation function (950 down to 600 keV/u). In addition, stable ^{48}Ti beam was used at four energies ($E_{\rm Ti}$ = 537, 702, 826 and 934 keV/u) to measure charge-state distributions of Ti. In the entire campaign of four beam times we could measure the excitation function ranging from $E_{\rm beam}$ = 605 to 1153 keV/u with 97 energy steps. With a total of 6.8×10^{15} ^{40}Ca atoms on target we could detect more than 5500 ^{44}Ti recoils.

Summary of the measurement at DRAGON

The goal of this experiment was to measure directly the ^{44}Ti production by α capture on ^{40}Ca over a wide temperature regime which is relevant for nucleosynthesis in the α-rich freeze-out, i.e. $T_9 \sim$ 1–2.8. The measurement has been performed in inverse kinematics with a ^{40}Ca beam with energies of 600 to 1200 keV/u.

High-purity ^{40}Ca beam (less than 0.5% ^{40}Ar contamination) was produced in a microwave ion source by sputtering from a Ca target. In order to meet the requirements of the ISAC accelerators ($A/q < 30$), the 2+ charge state was employed. Up to ∼100 enA of $^{40}Ca^{2+}$ were extracted and first accelerated to 150 keV/u with a room-temperature radio frequency quadrupole (RFQ) accelerator. After the beam passed through a thin carbon stripper foil, charge state 7+ was selected to accelerate the ^{40}Ca beam with a drift-tube linac (DTL) to the required energies. Typical currents on target were around 10 enA.

The recoil mass spectrometer DRAGON consists of a windowless gas target followed by a two-stage spectrometer based on magnetic and electrostatic dipoles with magnetic quadrupole and sextupole elements for focusing. The recoils are finally detected in an ion chamber equipped with a thin entrance window and a segmented anode for isobaric identification. The gas target is surrounded by a high-efficiency γ-ray detector array consisting of 30 BGO scintillators. In order to improve the identification of the ^{44}Ti recoils, we use a coincidence between γ-ray detection at the BGO array and heavy-ion detection at the ion chamber. Additionally, a narrow time-of-flight window and cuts on energy-loss signals allow a clear identification of the ^{44}Ti recoils. Because of the higher masses involved in this reaction, we had to add a thin 100 nm silicon nitride foil after the gas target (called the charge-state booster (CSB) foil) in order to reach high enough charge states to be bent by the spectrometer.

The yield of ^{44}Ti, which is the number of recoils per incoming projectile, is measured as a function of initial beam energy and gas-target thickness:

$$Y = \frac{N_{^{44}\rm Ti}}{N_{^{40}\rm Ca}\ F_q\ \epsilon}\ .$$

$N_{^{44}\rm Ti}$ denotes the detected recoils in a particular charge state and in most cases in coincidence with a high-energy γ-ray detected at the BGO array (called here "coincidences" as opposed to "singles" which means recoil detection only). The number of incoming beam particles $N_{^{40}\rm Ca}$ is calculated based on detection of elastically-scattered He atoms in a solid-state detector placed at 57° and normalization to an upstream Faraday cup. Corrections for the charge-state fraction of the recoils F_q and the detection efficiency ϵ have to be considered as well. The quantity ϵ includes the transmission through the spectrometer and the efficiency of the end detector; both are close to 100%. For coincidences, ϵ also includes the efficiency of the BGO-detector array.

Based on the measured yield, a resonance strength $\omega\gamma$ can be calculated:

$$\omega\gamma = \frac{2}{\lambda^2}\frac{m_t}{m_p + m_t}\left(\frac{dE}{dx}\right)Y$$

with λ as the de Broglie wavelength of the reduced mass of the compound system, m_p and m_t are the masses of projectile and target, and dE/dx is the stopping power per atom/cm^2 of the projectile in the target.

Charge-state distributions (CSD) of the ^{44}Ti recoils have been measured with a stable ^{48}Ti beam at four energies which cover the same velocity (or energy-per-nucleon) range. Due to limitations of the bending magnet, only the high charge states of the CSD were accessible. Figure 1 shows the CSD of the ^{44}Ti recoils at the strong resonances near 1130 keV/u (corresponding recoil energy of 920 keV/u) and compared with the CSD measured with stable beam at different gas pressures (both with the CSB foil). The slight change between the different pressures is caused by a small fraction of gas leaking behind the foil, enough to shift the CSD a little bit towards lower values. Figure 2 shows the charge-state fraction as function of gas-target pressure. At this energy, charge-state equilibrium is reached around 1.5 Torr which corresponds to ∼4 μg/cm^2.

Depending on the pressure in the gas target, the beam loses between 2.8 keV/u at 1 Torr (corresponding to a target thickness of 2.9 μg/cm^2) and 22.8 keV/u at 8 Torr. In order to cover the large energy range with a reasonable resolution, we decided to measure most of the time with a pressure of 4 Torr. The energy steps were chosen to overlap slightly in order not to

miss any narrow resonances. At lower energies (below 850 keV/u) we decided to measure at 8 Torr and without the CSB foil. This was motivated because at the lower energies the most probable charge states with the CSB foil are close to 11+, where beam suppression in the spectrometer is strongly reduced because of A/q ambiguities; without the CSB foil we could measure at 9+ and 10+. However, more overlap was necessary because a target thickness of 3–4 μg/cm^2 is necessary to reach charge-state equilibrium (see Fig. 2). This is important, otherwise the charge-state distribution would depend on the position of the reaction along the path in the gas target; ^{44}Ti recoils which originate from a reaction at the first section of the gas target (i.e. at the higher section of the covered energy range) are likely to reach charge-state equilibrium, whereas ^{44}Ti recoils from reactions near the end of the path in the gas target (i.e. at the lower section of the energy range) pass through less gas and thus result in a different CSD. This effect is not present if the CSB foil is used since the CSB foil "resets" the CSD independent of the incoming charge states.

Preliminary results

First tests were performed at strong resonances (an isospin triplet at $E_x = 9.2$ MeV) at a beam energy of 1130 keV/u, which had been measured several times in the past by prompt γ-ray spectrometry and off-line counting using AMS. The high yield allowed measurements at several charge states (12+ to 16+) and a clear signal in the singles spectrum was observed. Thus, a direct determination of the resonance strength was possible. With a measured summed resonance strength for the isospin triplet of $\sum\omega\gamma = 7.7 \pm 0.7$ eV [Vockenhuber *et al.*, Nucl. Instrum. Methods B, in press], a good agreement with the previous measurements was found.

Figure 3 shows the preliminary excitation function of the entire energy range. Each horizontal box (blue) indicates the covered energy range in the x direction and the yield in the y direction with the error as a vertical line at the centre energy. Previously known resonances (with a known resonance strength) are shown as vertical bars (red). Not included in our data for this plot are the full analyses of the CSD and BGO efficiencies based on γ-ray data. However, the DRAGON data clearly show ^{44}Ti yields at energies between known resonances. Note, excitation functions shown in the literature of the prompt γ-ray spectrometry indicate some yield between these resonances, but it is not clear if this yield originates from instrumental background or reactions with contaminants; commonly used reaction rates are based on adaption of statistical model codes to these known resonances.

Our study results in a higher summed yield compared to the summed yield of known resonances from the prompt γ-ray measurements and confirms – at least to some extent – the finding of the integral measurement using AMS. A detailed analysis including the γ-ray data is nearing completion.

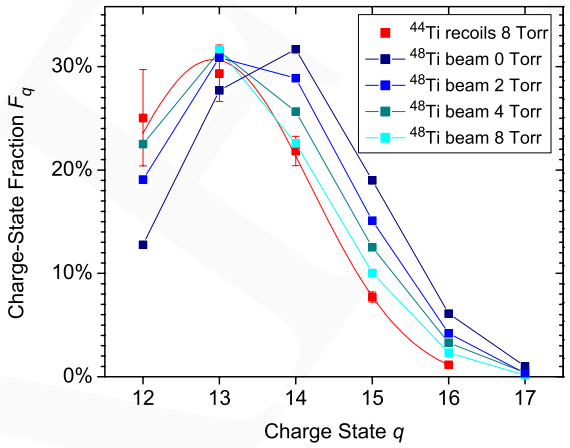

Fig. 1. Charge-state distribution of Ti at 920 keV/u after the CSB foil measured with ^{44}Ti recoils (red) at 8 Torr and ^{48}Ti beam (blue shades) at different gas pressures.

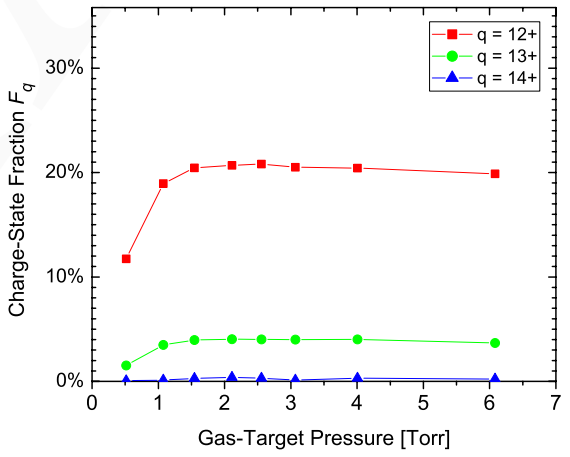

Fig. 2. Charge-state fractions of Ti at 920 keV/u without the CSB foil as a function of gas target pressure measured with a ^{48}Ti beam.

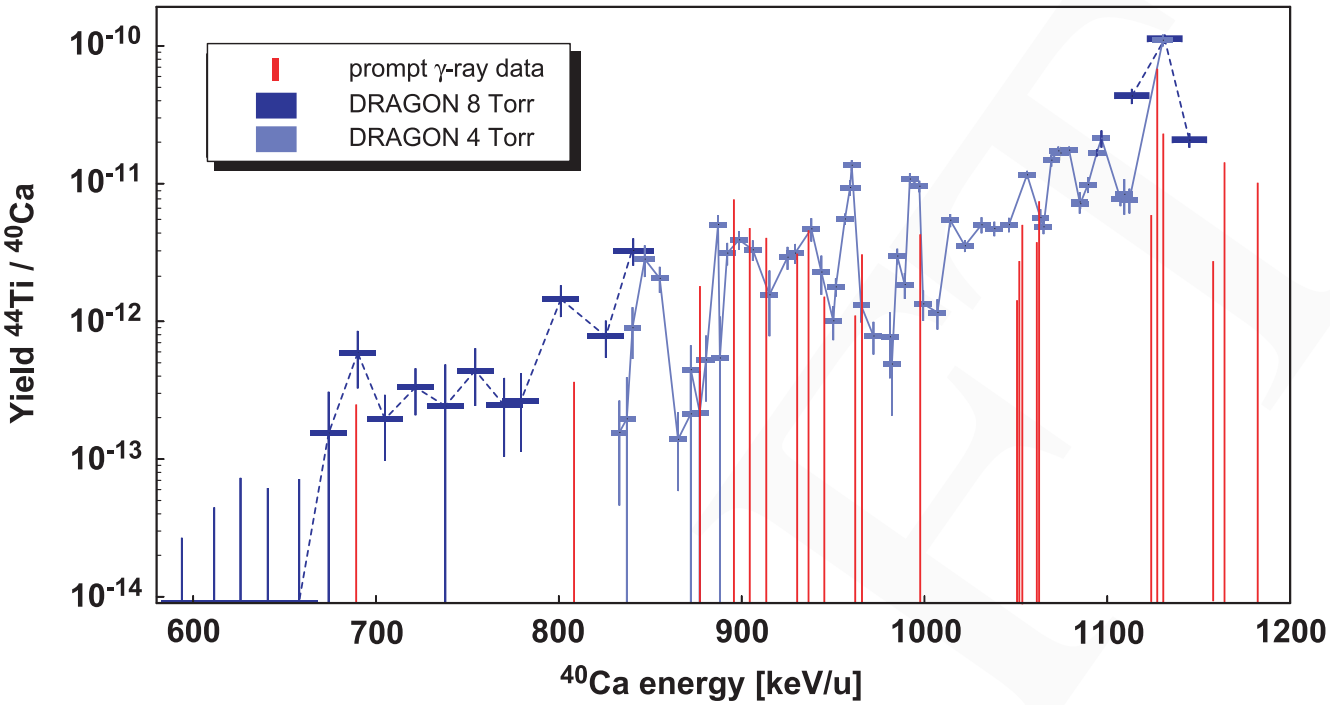

Fig. 3. Preliminary excitation function of the ^{40}Ca$(\alpha,\gamma)^{44}$Ti reaction measured at DRAGON. Data sets at 4 Torr and 8 Torr are indicated in different blue shades, the connecting lines are only to guide the eye. The yield at each measurement point depends on how many narrow resonances are hit, thus overlapping bars at different pressures agree with each other only if the same resonances are hit in both cases. For comparison, vertical red lines indicate known resonance strengths from prompt γ-ray studies.

Experiment 1027
Measurement of the ^{22}Na$(p,\gamma)^{23}$Mg reaction rate
(C. Ruiz, TRIUMF)

Radioactive ^{22}Na ($t_{1/2}$ = 2.6 yr) is one of the promising candidates for so-called diagnostic γ-rays; characteristic signatures of a particular isotope's production in astrophysical environments such as novae and supernovae. ^{22}Na is thought to be produced in some abundance in novae, and because of its relatively short half-life (on astronomical timescales), enough flux of γ-rays characteristic to this isotope (E_γ = 1.275 MeV) might be present allowing detection by an orbiting observatory such as INTEGRAL. Such a measurement would provide a solid basis for comparison between real nova events and numerical simulations including advanced nucleosynthesis networks.

So far, no γ-rays characteristic of ^{22}Na have been detected during observation of an individual nova event (using the Compton Gamma Ray Observatory). Given the current accepted model prediction for the amount of ^{22}Na made in these events, it is thought that the novae observed so far are well outside the flux detection limits in terms of distance. In order to observe decaying ^{22}Na we need a nova to occur much closer to our solar system. However, these predictions are based on the current knowledge of the reactions which create and destroy ^{22}Na in novae. Of prime importance is the reaction ^{22}Na$(p,\gamma)^{23}$Mg which directly destroys ^{22}Na. In general the stronger this reaction is, the less ^{22}Na abundance will result in the expanding nova shell.

Recently a new level was found in the nucleus ^{23}Mg using brute-force γ-ray spectroscopy [Jenkins *et al.*, Phys. Rev. Lett. **92**, 031101 (2004)] at E_x = 7.769 MeV. This would correspond to a low-energy resonance in the ^{22}Na$(p,\gamma)^{23}$Mg reaction at E_R = 189 keV which could substantially change the reaction rate. Indeed, estimates of the strength of this resonance suggest that it could be the *dominant* contribution to the rate at typical nova temperatures. A direct measurement of this resonance strength is therefore crucial to understanding O-Ne nova observations and models.

The DRAGON group at TRIUMF have initiated a project to measure this resonance strength in collaboration with the Nuclear Physics Group at the University of Washington, Seattle. Using the high-intensity ^{22}Na beams available at TRIUMF, implanted targets of 300 μCi and 185 μCi activities were fabricated in late 2005, as reported in the 2005 Annual Report. These correspond to ^{22}Na areal densities of 1.3×10^{15} atoms/cm^2 and 8.1×10^{14} atoms/cm^2 respectively. The more dense target will be used for the final experiment, and both targets will be used to test the experimental set-up. The Three Stage 9 MV Van

de Graaf Accelerator at the University of Washington will allow up to 50 μA of rastered proton beam to be impinged on the ^{22}Na targets during the experiment.

In 2006, in parallel with the construction of a new purpose-build beam line at the University of Washington accelerator facility, the DRAGON group began the design and construction of a new target chamber in order to perform the experiment. This chamber has several features crucial to the final measurement. Firstly, the chamber is constructed so as to present only LN_2 cooled surfaces to the target, acting both to discourage thermal migration of ^{22}Na and clean up the vacuum preventing contaminant build-up on the target surface. Also, the target will be backed by a water-cooled plate allowing efficient conduction of heat deposited by the intense proton beam that will be used in the experiment. Several diagnostic devices have been included in the chamber including a collimator ladder and current readout from the target plate. Electron suppression from the target surface is also a feature. Minimum surface is presented to the two HPGe detectors that will be used in the experiment, and the whole system has been designed with clean, UHV in mind. The targets will be transported in specially designed holders which will function not only as storage for targets not in use, but also as the cooled target block in the experiment itself, ensuring minimum handling and maximum safety.

The DRAGON group have also begun work into assembling a data acquisition system capable of obtaining high precision and efficiency at high count rates. Possibly a set of fast digitizing cards will be used to record such features as beam raster patterns as well as allowing intelligent trigger conditions/background rejection.

It is expected that the experiment will be ready to run in the summer, 2007 when the Seattle beam line and target chamber are completed.

Experiment 1031
Charged particle exit channels from the ^{12}C+^{12}C fusion reaction at astrophysical energies

(A.M. Laird, York; M. Aliotta, Edinburgh)

Motivation

The ^{12}C +^{12} C fusion reaction is important in explosive carbon burning in type 1a supernovae as well as in hydrostatic burning during standard stellar evolution. At the relevant temperatures in both scenarios, ($0.8 - 1.2 \times 10^9$ K), the reactions ^{12}C(^{12}C, p)^{23}Na and ^{12}C(^{12}C, α)^{20}Ne dominate, resulting in the main products of carbon burning being ^{20}Ne and ^{24}Mg (from ^{23}Na(p, γ)^{24}Mg and ^{20}Ne(α, γ)^{24}Mg).

Consequently, not only is the ^{12}C +^{12} C fusion rate important for describing stellar evolution subsequent to helium burning, but it also dominates the ignition of thermonuclear runaway leading to type 1a supernovae. Measurements which yield information on the astrophysical S-factor at temperatures between $0.8 - 1.2 \times 10^9$ K, corresponding to a centre of mass energy range of 1 to 3 MeV, are therefore highly important.

Experiment

After technical difficulties encountered (detectors and beam delivery) in the initial study in 2005 (see 2005 Annual Report), TUDA performed further experimental measurements in April 2006 for a feasibility study of the proposed technique for low energies. This was achieved by measuring an energy region covered by existing data [Becker *et al.*, Z. Phys. **A303**, 305 (1981)].

A $^{12}C^{3+}$ beam was provided by OLIS with a maximum intensity of around 55 enA. The beam energy was varied between 670 keV/u ($E_{\rm cm} = 4.02$ MeV) and 566 keV/u ($E_{\rm cm} = 3.4$ MeV). As previously, the beam energy was measured using DRAGON, before and after each energy change, to determine the beam energy with high accuracy and to ensure that the beam energy had not drifted during the course of a run. This is extremely important due to the sensitivity of the cross section to the centre of mass energy. Enriched carbon targets of thickness 20 μg/cm^2 were used. The experimental set-up (see 2005 Annual Report) comprised two LEDA-type silicon strip detectors (1000 μm and 300 μm thickness) and one S2-type detector (500 μm). The forward detector arrays were protected from elastic scattering by aluminum foil with the exception of the monitor detector. One LEDA detector was offset upstream to cover the angular region around 45°. This detector had five 1 mm holes in the shield, at each of five angles, to provide elastic scattering data around 45° for normalization purposes. Four photodiodes were also included in the set-up to provide further monitoring at larger (about 50°) angles. The previous experimental run in July 2005 had demonstrated the necessity of protecting the detectors from beam induced electrons and so all detectors were "shielded" by a bias of +3 kV.

Figure 1 shows on-line data for an angle of 19° and beam energy of 652.5 keV/u ($E_{\rm cm} = 3.9$ MeV), acquired over a period of approximately 14 hours. Detailed analysis of the data is ongoing to calculate angular distributions, for each reaction, at each energy step. The results will then be compared to published data. However, initial results suggest that contamination in the targets, both hydrogen and heavy elements, will limit this technique to the extent that such measurements in the astrophysically important region will not yield reliable data. However, it is anticipated that

the current data from our charged particle experiments will provide a useful test of recent γ-based measurements, and alternative techniques for such studies are currently being investigated using e.g. TACTIC (see this Annual Report).

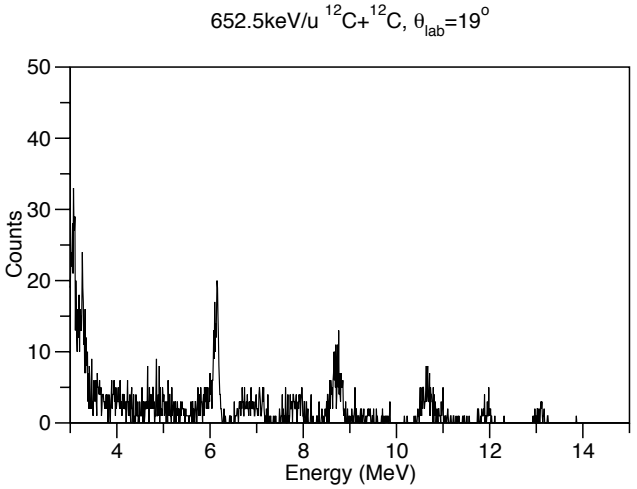

Fig. 1. On-line data at 19° in the lab (LEDA1) which includes both proton and alpha events.

Experiment 1056
Precise determination of the ^{8}Li valence neutron ANC: testing mirror symmetry and the ANC method in astrophysics
(B. Davids, TRIUMF)

Recently, the nuclear physics community has shown intense interest in asymptotic normalization coefficients (ANCs). Many measurements of ANCs in transfer reactions with light and heavy ions have been performed, including quite a number with radioactive beams. Most of these measurements are motivated by the goal of determining astrophysical reaction rates indirectly. For many non-resonant (p,γ) and even some (n,γ) reactions important in stars, the radiative capture occurs well outside the nuclear interior. The rates of these reactions are therefore determined by the probability of finding the valence nucleon at large distances. This probability is given by the ANC, which is the normalization of the tail of the overlap integral between the wave functions of the target and recoil nuclei. The ANC uniquely determines the astrophysical S factor of charged-particle induced radiative capture reactions at zero energy. By exploiting this relation, the astrophysical S factor for the important ^{7}Be$(p,\gamma)^8$B reaction, $S_{17}(0)$, has been derived from measurements of (^{7}Be,^{8}B) transfer reactions. Although much effort has been expended in recent years to determine $S_{17}(0)$, both directly by means of radiative capture measurements and indirectly via Coulomb breakup and ANC measurements, the situation is still somewhat confused. The most recent radiative capture measurement is by far the most precise measurement and therefore dominates weighted averages. However, it is curious that the other low energy radiative capture measurements and the indirect measurements agree quite well and imply a lower value for $S_{17}(0)$.

ANCs are usually determined by analyzing transfer reaction data in the framework of the distorted wave Born approximation (DWBA). For these analyses to be valid, two conditions must hold true. First, the reaction must be peripheral, so that poorly known contributions from the nuclear interior do not affect the ANC derived from the measured cross section. Second, the interaction mediating the reaction must be weak enough that multi-step corrections to the DWBA analysis are small. In addition to these two conditions, there is a third requirement that has received less attention. The DWBA transition amplitude for the transfer reaction contains a remnant term which is not proportional to the ANC. In the prior form, the DWBA transition amplitude takes the form

$$T_{fi} = \int\int \chi^{(-)}(\mathbf{k_b},\mathbf{r_b})^* \langle \Psi_{^8Li}\Psi_{^7Li}|(V_{n^7Li} + V_{^7Li^7Li} - U_{^7Li^8Li})|\Psi_{^7Li}\Psi_{^8Li}\rangle \chi^{(+)}(\mathbf{k_a},\mathbf{r_a}) d\mathbf{r_a} d\mathbf{r_b},$$

where $\chi^{(-)}(\mathbf{k_b},\mathbf{r_b})$ and $\chi^{(+)}(\mathbf{k_a},\mathbf{r_a})$ are the distorted waves in the exit and entrance channels. The difference between the core-core interaction and the ^{7}Li-^{8}Li optical potential, $V_{^7Li^7Li} - U_{^7Li^8Li}$, is known as the remnant term. If it is not negligibly small, this term destroys the proportionality between the DWBA cross section and the ANC. All recent DWBA analyses of transfer reactions have implicitly assumed that the remnant term can be factored in this way and that the ANC can be inferred from the overall constant by which the theoretical DWBA calculation is scaled to match the experimental cross section. In such experiments, particularly those involving heavy ions, the effect of the remnant term on the inferred ANCs is not clear.

Recent theoretical work shows that the charge symmetry of the strong interaction implies a relation between the ANCs of the one-nucleon overlap integrals in light, mirror nuclei. This relation has been used to deduce the ANC for ^{8}B $\rightarrow^7$Be$+p$ from the ^{8}Li $\rightarrow^7$Li $+n$ ANC. The results of this ANC determination from a neutron transfer reaction were in good agreement with the results of prior proton transfer reactions in the isospin mirror system. Both of these ANC determinations imply values of $S_{17}(0)$ that are considerably smaller than the recent, high precision direct measurement of the low energy radiative capture cross section. It is important to ascertain if the low values of $S_{17}(0)$ implied by the ANC determination can be confirmed

by an independent ANC measurement in the isospin mirror system.

We have endeavoured to measure the ANC of the valence neutron in ^{8}Li by measuring the elastic transfer reaction ^{7}Li(^{8}Li,^{7}Li)^{8}Li at two beam energies, 11 and 13 MeV. By measuring a transfer reaction with identical initial and final states, we take advantage of several important facts. First, the vertex of interest appears twice in the reaction, so we can improve the statistical precision of the ANC determination relative to a reaction that involves two distinct vertices. Second, we need only consider a single target-projectile interaction, limiting the uncertainties due to optical potentials. Finally, by measuring elastic scattering simultaneously, we can determine the optical model parameters that are the single largest reported source of uncertainty in ANC determinations from transfer reactions. At these energies near the Coulomb barrier, we expect the reaction to be peripheral, and that multi-step effects are small. By measuring the inelastic excitations of ^{8}Li to its first 1^+ excited state we will also measure its ANC and test charge symmetry for this state.

The interference between elastic scattering and neutron transfer produces characteristic oscillations in the differential cross section as a function of the scattering angle. By analyzing the amplitudes of the interference minima and maxima, we can determine the ANC for ^{8}Li $\rightarrow^7$Li $+n$. It is essential to ascertain the effect of the remnant term in order to precisely infer the ANC and test previous ANC analyses based on the DWBA. We will accomplish this by carrying out the measurement at two beam energies. Since the first part of the remnant term, $V_{^7Li^7Li}$, is independent of energy, measurements at more than one energy will allow us to determine the optical potential, the remnant term, and the ANC unambiguously and with high precision. Moreover, measuring at two energies gives us redundant information in case one of the energies coincides with a resonance in the compound nucleus, ^{15}C. In conjunction with previous measurements, this experiment will allow us to test mirror symmetry in the A = 8, T = 1 system and assess the validity of the ANC method for determining astrophysical S factors. Provided we find no problem with the method, we will use the ANC and charge symmetry to infer the astrophysical S factor for ^{7}Be(p,γ)^{8}B reaction, $S_{17}(0)$.

Experiment 1056 was performed in the TUDA chamber in the ISAC hall of TRIUMF. Two highly segmented silicon detectors were used to cover the desired angular range. A Micron S2 detector consisting of 48 concentric rings and 16 sectors was used to cover centre of mass angles from 10–30°, while a LEDA detector composed of 8 sectors, each with 16 rings, was used to cover the centre of mass angles from 70–122°. These detectors were used to detect ^{7}Li and ^{8}Li nuclei.

The experiment collected data between July 21 and 25. A total beam time of roughly 86 hours was logged with an average rate of 1800 good events per second. The average ^{8}Li beam intensity was 2×10^7 s^{-1}. SFU M.Sc. student Derek Howell is analyzing these data within the ROOT data analysis framework. The use of the TUDAROOT software developed at TRIUMF has facilitated the conversion from the MIDAS tarball data format into the tree data format used by ROOT. Currently, the analysis is focused on the calibration of the LEDA and S2 detectors and kinematic angle-energy correlation checks.

Experiment 1057
Spectroscopy of ^{9}Li
(R. Kanungo, St. Mary's Univ.)

The modification of shell structure for neutron-rich nuclei has motivated extensive research on the search for new magic unstable nuclei. In an earlier work on systematic studies of nuclear binding, it was shown that N = 6 exhibits the signature of a closed shell [Kanungo *et al.*, Phys. Lett **B528**, 58 (2002)] for neutron-rich isotopes of He, Li, Be. The shell model calculation of Otsuka *et al.* also predicts this shell closure [Phys. Rev. Lett. **87**, 082502 (2001)].

At the ISAC facility at TRIUMF we have investigated the ground state structure of ^{9}Li, the N = 6 isotone through the one neutron transfer reaction $d(^9\mathrm{Li},t)^8$Li at $E \sim 1.7$ A MeV. The results obtained show the ^{8}Li subsystem inside ^{9}Li to be populated in its different excited states. This shows that the ^{9}Li nucleus is composed of a superposition of different configurations with ^{8}Li in its different excited states coupled to a neutron in the p orbital.

The experiment was carried out at the TUDA beam line in ISAC-I. The radioactive beam of ^{9}Li with an average intensity of $\sim 10^5$/s was incident on a 100 μg/cm^2 thick deuterated polyethylene $(CD_2)_n$ target. The scattered tritons and the ^{8}Li nuclei were detected using annular silicon strip detectors. The 1 mm thick LEDA detectors (a large area silicon array with the active outer radius of 129 mm and active inner radius of 50 mm) placed 11 cm downstream of the target detected the tritons in the angular range of 24–49° in the laboratory. The ^{8}Li nuclei after the (d,t) reaction were detected using a smaller silicon array, the S2 detector, placed 13 cm downstream of the target (Fig. 1a). The combined angular coverage of both detectors allowed us a wide coverage of centre-of-mass angles for $d(^9\mathrm{Li},t)^8\mathrm{Li}_{\mathrm{gs}}$. The detection of tritons and ^{8}Li in coincidence in these two detectors served a useful way of eliminating background channels and obtaining a better view of some excited states in ^{8}Li (Fig. 1b). The

data analysis is in progress to extract the angular distributions for the different states of ^{8}Li.

In order to extract the spectroscopic amplitudes of the different configurations constituting the ground state of ^{9}Li we will be performing a DWBA analysis of the experimental angular distributions. This requires a knowledge of optical potentials. To this end in the same experiment we measured the elastic scattering ^{9}Li and ^{8}Li with the $(CD_2)_n$ target. The elastic scattering angular distributions provide us guidance of the optical potentials.

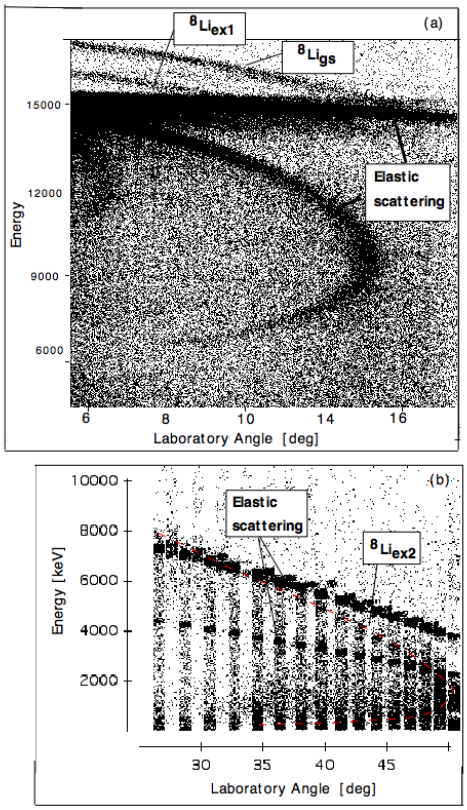

Fig. 1. The kinematic loci of the data for particles in (a) the S2 array and (b) the LEDA array events in coincidence with the S2 array. The elastic scattering loci in (a) are scattering from both C and deuteron in the target. The vertical bands seen in (b) represent the different strips of the LEDA detector.

Experiment 1058
Coulomb excitation of radioactive ^{20,21}Na
(M.A. Schumaker, Guelph)

Experiment 1058, the first radioactive beam experiment using high-purity germanium (HPGe) detectors from the TRIUMF-ISAC gamma-ray escape-suppressed spectrometer (TIGRESS) array, has been performed successfully. The experiment used two TIGRESS detectors, and accelerated radioactive ion beams from ISAC-I in July–August. This experiment studied the structure of the mirror nuclei ^{21}Ne and ^{21}Na; both nuclei with Five valence nucleons outside an ^{16}O core. This configuration is relevant to our understanding of the five particle, two hole configuration of the astrophysically-important $3/2^+$, 4.033 MeV excited state of ^{19}Ne. This is the dominant γ-ray emitting level in the ^{15}O$(\alpha,\gamma)^{19}$Ne reaction, thought to be responsible for the breakout from the hot CNO cycle into the rp-process in X-ray bursting neutron stars [Wiescher *et al.*, J. Phys. **G25**, R133 (1999)]. While these nuclei have previously been studied using nuclear reactions and β-decay studies, neither has been studied by Coulomb excitation, and thus the B(E2) values have never been directly measured. For these odd-A nuclei, for which M1 γ decay is dominant, the preferential selection of E2 excitation provided by Coulomb excitation is very important. For example, in ^{21}Na, the presently accepted B(E2) value for the transition from the $3/2^+$ (5p) ground state to the $5/2^+$ state has an uncertainty of $\pm$86%. The increased precision provided by the current experiment will allow this B(E2) value to be used as a stringent test of the shell model's ability to describe the structure of 5p states in this region.

For approximately one week, ^{21}Ne was produced by OLIS at a rate of $\sim 5 \times 10^6$ ions/s. These ions were accelerated to 1.7 MeV/u on the ISAC-I high-energy line, and Coulomb excited using a $\sim$1 μm ^{nat}Ti target. A radioactive ^{21}Na beam was then produced and accelerated at a similar intensity for an additional week.

The apparatus used to detect scattered particles and de-excitation γ-rays is shown in Fig. 1. Beam particles (arriving from the lower right) scattered from the ^{nat}Ti target within the target chamber constructed at the University of Rochester, and were detected by the BAMBINO 24 $\times$ 16-segmented silicon CD detector, developed by Lawrence Livermore National Laboratory. The BAMBINO detector covered scattering angles from 20 to 50°. Detection of scattered target particles allowed a range of beam particles scattered at backward angles to be observed as well. Two TIGRESS detectors perpendicular to the beam axis (upper right, and lower left of Fig. 1) were used for γ-ray detection.

All 160 electronic channels were read out to the TIG-10 digital electronics modules, newly developed at the Université de Montréal. A plastic scintillator provided by the Université de Laval, located 1.2 m downstream from the target chamber, was used to monitor the beam intensity during the measurements.

For each beam, Coulomb excitation from the $3/2^+$ ground state to the $5/2^+$ state was observed, producing 350.7 keV and 331.50 keV γ-rays for ^{21}Ne and ^{21}Na, respectively. Figure 2 shows the resulting γ-ray spectrum for each beam, with a preliminary Doppler correction applied. For each beam, normalizing the γ-ray intensity using the $0^+ \rightarrow 2^+$, 983.5 keV transition in

the ^{48}Ti target as a reference will result in an accurate measurement of the B(E2) values. The analysis of these data is currently in progress.

After the success of this first experiment, a more difficult experiment was attempted; the Coulomb excitation of the proton dripline nucleus ^{20}Na, for which no γ-ray transition matrix elements have been measured previously. The ^{20}Na beam was also accelerated to 1.7 MeV/u, and the same target and apparatus were used. This nucleus is of interest due to its role in the initiation of the rp-process through the $^{15}\mathrm{O}(\alpha,\gamma)^{19}\mathrm{Ne}(p,\gamma)^{20}\mathrm{Na}$ reaction chain, though only recently has its level structure below the proton emission threshold been determined at the Argonne stable beam facility [Seweryniak *et al.*, Phys. Lett. **B590**, 170 (2004)].

The yield available from ISAC was more than sufficient for the experiment, and a beam of $\sim 5 \times 10^6$ ions/s was delivered. The remaining challenges involved in determining B(E2) values for this nucleus are the result of its short β^+ lifetime, and the subsequent α decay of an excited state of its daughter, ^{20}Ne. The background γ and particle counts are significant, though these can be limited through different background suppression and subtraction techniques. The progressive improvement in the resulting γ-ray spectra is shown in Fig. 3. In Figure 3a, the γ-ray spectrum for Si-γ coincidence, the dominant feature in the spectrum is the peak resulting from the 511 keV annihiliation γ-rays, which obscures all other features. Establishing time gates on the coincidence, and gating on the energy of the Si energy (removing counts due to α particle detection), as shown in Fig. 3b and Fig. 3c, respectively, results in enough improvement to identify the 199 keV, 599 keV, and 799 keV deexcitation γ-rays for the $4^+ \rightarrow 3^+$, $3^+ \rightarrow 2^+$ (ground state), and $4^+ \rightarrow 2^+$ transitions, respectively, in ^{20}Na. Further improvements resulting from applying Compton suppression, and the subtraction of random Si-γ events are shown in Fig. 3d and Fig. 3e. The number of counts observed for each of these γ-rays will be sufficient to determine, for the first time, B(E2) values for this proton-dripline nucleus.

The analysis of the Expt. 1058 data is proceeding. The success of this experiment has provided a very positive outlook for future experiments with additional TIGRESS detectors, at higher energies, and heavier nuclear masses at ISAC-II.

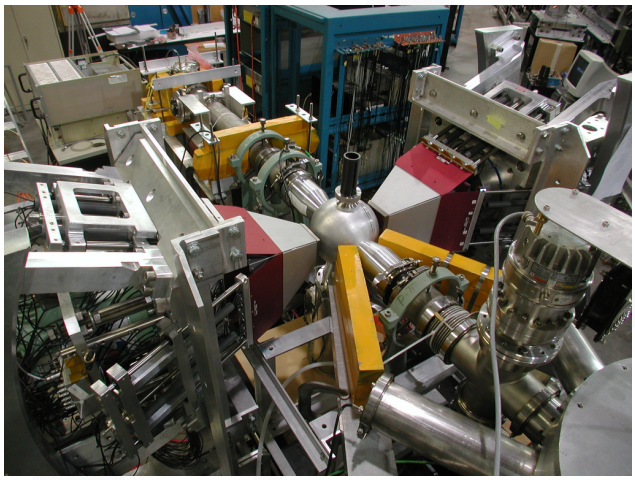

Fig. 1. Two TIGRESS detector modules used for Expt. 1058.

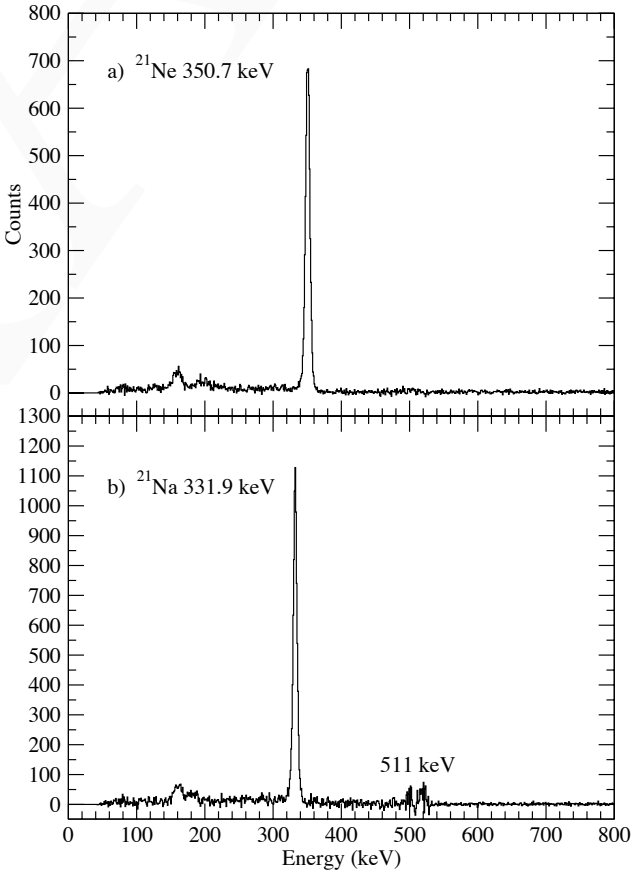

Fig. 2. a) ^{21}Ne and b) ^{21}Na γ-ray spectra.

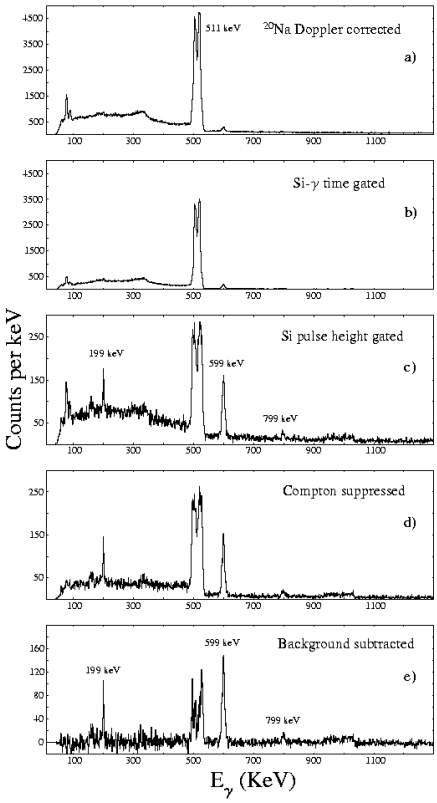

Fig. 3. Background suppression in ^{20}Na γ-ray spectra. See text for details.

Experiment 1061
Effect of ortho-para ratio on muon catalyzed fusion in gas/liquid/solid deuterium
(H. Imao, K. Ishida, RIKEN; N. Kawamura, KEK)

The resonant muonic molecular formation plays an essential role in muon-catalyzed fusion (μCF) because it primarily determines how many fusion reactions occur within a muon lifetime of 2.2 μs. Our group has experimentally investigated the resonant $dd\mu$ formation in the solid, liquid and gas phases while controlling the ortho-para ratio of deuterium, where the distribution of the initial rotational state, K_i, of D_2 molecules was controlled by changing the ortho-para ratio. In the previous experiment (Expt. 968), we found that the resonant $dd\mu$ formation rate, $\tilde{\lambda}_{\frac{3}{2}}$, and the $d\mu$ hyperfine transition rate, $\tilde{\lambda}_{\frac{3}{2}\frac{1}{2}}$, in ortho-$D_2$ were lower than those in normal-D_2 both in the solid and liquid phases. In the gas phase, a delayed bump structure with overlapping exponential spectrum was found only in the spectra for ortho-D_2. The fusion neutron yield was increased in ortho-D_2 because of the bump structure. The aim of Expt. 1061 was to study the ortho-para dependent phenomena near the liquid/gas boundary to determine the nature of the condensed-matter effect. In addition, the measurements with para-enriched D_2 were performed in order to determine the origin of the structure.

We measured the emission-time distribution of *d-d* fusion neutrons from ortho-para controlled deuterium both in liquid (ϕ = 0.86–1.16, T = 23.2–35.0 K) and gas (ϕ = 0.03–0.17, T = 36.2 K) phases. A cross sectional view of the experimental set-up is shown in Fig. 1.

We changed the μ^- beam momentum in the range of 48–52 MeV/c for different target densities. Four NE-213 liquid scintillators (ϕ 5 in. × L 2 in., N1–N4) around the deuterium target had a large solid angle (40%) for detecting 2.5 MeV *d-d* fusion neutrons. We used two types of bullet-shaped target cells made of oxygen-free high-conductivity (OFHC) copper for gas and liquid targets, respectively. These cells were sufficient to sustain the maximum operating pressure of 12.2 bars. We used para-rich (50 and 55% ortho), normal (66% ortho) and ortho-rich D_2 (90 and 99% ortho). Para-rich D_2 gas was produced by using the preferential adsorption method. As an adsorbent, we used grained γ-alumina powder (∼3 mm), which was filled in an OFHC copper cell at a temperature of 30 K. By keeping normal-D_2 gas flowing through the adsorbent, 55% ortho-D_2 gas was collected. Gas analysis using the Raman spectroscopy method was carried out before and after each experimental run to check that the ortho-para ratio was not changed during the run.

In the liquid phase, the ortho-para dependence on the resonant $dd\mu$ formation rate $\tilde{\lambda}_{\frac{3}{2}}$ in 28–35 K had a same tendency as that previously observed in 3.5–23.2 K (Fig. 2). We also observed that the rate for para-rich D_2 (ortho 55%) is higher than that for normal D_2 for the first time. In the gas phase, we confirmed the reproducibility of a delayed structure on the neutron time spectrum for ortho-D_2. A similar delayed structure was clearly observed also in the spectra at the lower target densities of $\phi = 0.03$ and 0.07. The amplitude of the structure proportionally depended on the ortho concentration. The structure difference between normal and para-rich D_2 was opposite to that between normal and ortho-rich D_2. Considering the clear ortho-para dependence in the delayed structure, the transient $dd\mu$ formation from $d\mu$ atoms in the thermalizing stage, which was ignored in the conventional analysis for *d-d* μCF, possibly causes the structure. The fusion neutron yield Y_n becomes higher with ortho-concentration increasing at all observed densities in the gas phase. We used the parameter δY_n defined as

$$\delta Y_n = \frac{1}{c_o^o - c_o^p} \cdot \frac{Y_n^o - Y_n^p}{Y_n^o + Y_n^p},$$

where c_o^o and c_o^p are the ortho concentrations for the ortho ($c_o^o = 0.99$) and para-rich or normal ($c_o^p = 0.50$, 0.55 or 0.66) targets that we used in the experiments and Y_n^o and Y_n^p are the fusion neutron yield per muon

for the ortho- and para-rich targets, respectively. As shown in Fig. 3, the ortho-para effect on the fusion neutron yield, δY_n, showed the opposite tendency between gas and liquid deuterium even at similar temperatures.

The result directly indicates the existence of strong density dependence of the ortho-para dependent phenomena. A detailed analysis to extract further information (e.g., the steady-state resonant $dd\mu$ formation rate in the gas phase taking the $d\mu$ slow thermalization into account) is in progress.

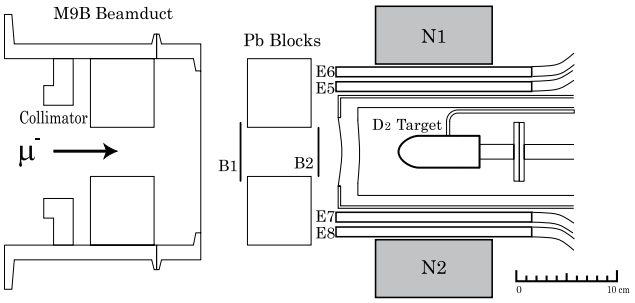

Fig. 1. Schematic view of the experimental set-up with pressurized liquid D_2 target.

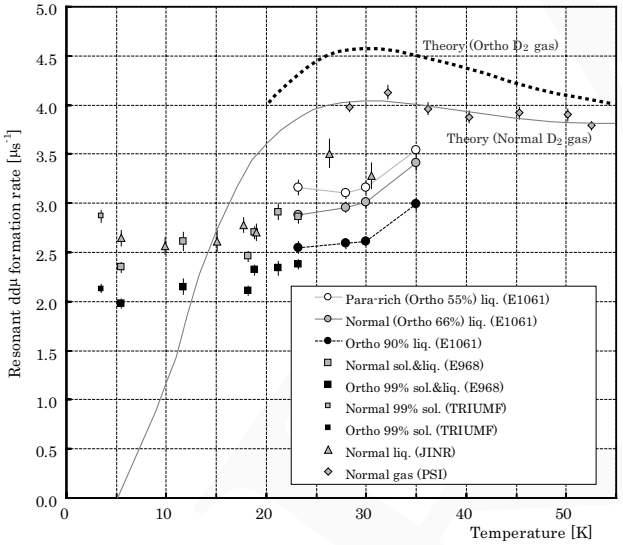

Fig. 2. The resonant $dd\mu$ molecular formation rate $\tilde{\lambda}_{\frac{3}{2}}$.

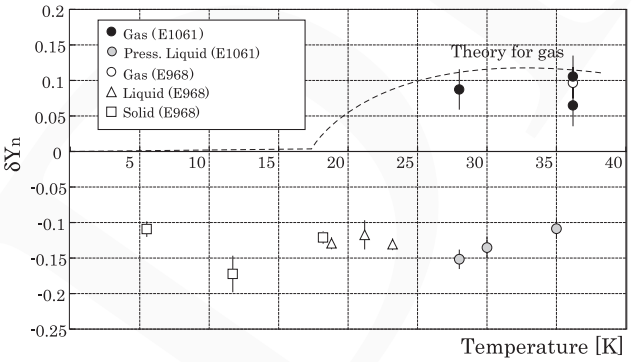

Fig. 3. Temperature dependence of the ortho-para effect on the fusion neutron yield.

Experiment 1064
Excited states in the Ca isotopes towards "doubly-magic" ^{54}Ca: decay of $^{51-53}$K
(R.V.F. Janssens, Argonne)

Shell model calculations with the new GXPF1 pf shell interaction [Honma *et al.*, Phys. Rev. **C65**, 061301(R) (2002)]. have suggested the development of significant sub-shell gaps at $N = 32$ and $N = 34$ in the Ca isotopes. These new gaps in these neutron-rich nuclei are believed to be the result of a reduced proton $f_{7/2}$–neutron $f_{5/2}$ monopole interaction as protons are removed from the $f_{7/2}$ orbital when the proton number decreases from $Z = 28$ (Ni) to $Z = 20$ (Ca). Confirmation of the $N = 32$ sub-shell gap has already been achieved in the Ti and Cr isotopic chains, based on the results of beta-decay measurements, high-spin state studies following deep inelastic reactions and B(E2) transition strengths through Coulomb excitation of intermediate energy fragments [Janssens *et al.*, Phys. Lett. **B546**, 55 (2002); Dinca *et al.*, Phys. Rev. **C71**, 041302(R) (2005); Zhu *et al.*, Phys. Rev. **C74**, 064315 (2006)]. However, there is no evidence for an $N = 34$ shell closure in ^{56}Ti and ^{58}Cr. For example, the energy of the first excited 2^+ state in ^{56}Ti [Liddick *et al.*, Phys. Rev. Lett. **92**, 072502 (2004)] falls midway between the shell model predictions with the GXPF1 Hamiltonian, where a shell closure is expected, and those with the KB3G interaction, where this gap is absent. However, the presence of a $N = 34$ shell gap at ^{54}Ca, where the proton $f_{7/2}$ shell is empty, cannot be ruled out. In fact, the latest calculations with a modified GXPF1 interaction, labelled GXPF1A, still predict a gap at $N = 34$ in the Ca isotopic chain [Dinca *et al., op cit*; Gade *et al.*, Phys. Rev. **C74**, 021303(R) (2006); Otsuka, private communication]. Systematic data on the approach to the proposed ^{54}Ca "doubly-magic" nucleus are critical to test the latest shell model predictions. To put it simply, with the $Z = 20$ proton shell closed, the neutron-rich calcium isotopes provide a unique opportunity to delineate neutron shell structure above $N = 28$. Specifically, information on the ordering and on the location of the $p_{3/2}$, $p_{1/2}$ and $f_{5/2}$ orbitals is highly desirable. In order to address the issue, a study of the $^{51-53}$Ca isotopes through the beta decay of mass selected $^{51-53}$K nuclei was undertaken at the ISAC facility.

The neutron-rich $^{51-53}$K isotopes were produced by spallation of a Ta target by 500 MeV protons, and extracted from a surface ionization source as singly-charged ions. The desired isotopes, following mass separation, were implanted into the moving tape collector located at the centre of the 8π spectrometer array of 20 escape-suppressed HPGe detectors and the SCEPTAR plastic scintillator array. These facilities are de-

scribed elsewhere in this Annual Report. The event-by-event coincidence data recorded for subsequent analysis included $\beta-\gamma$ and $\beta-\gamma-\gamma$ coincidences. β-gated, γ-single spectra and $\gamma-\gamma$ coincidence matrices have been analyzed for all three cases ($^{51-53}$K). Figure 1 is a spectrum obtained for ^{51}K. The detailed analysis is ongoing.

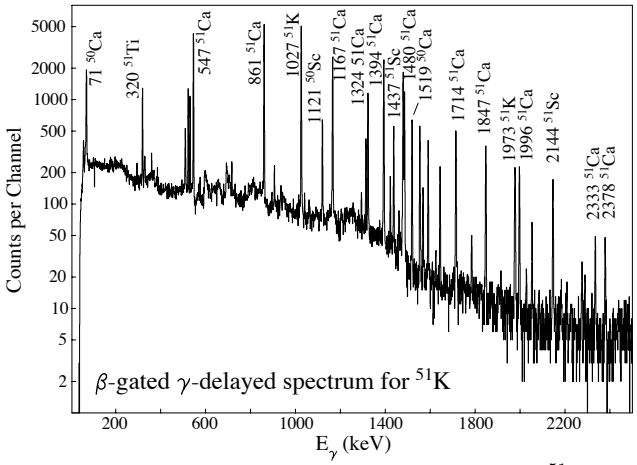

Fig. 1. *gamma*-ray spectrum from β-decay of ^{51}K.

Experiment 1070
Upgrade of ^{38m}K β-ν correlation

(J.A. Behr, C. Höhr, TRIUMF; A. Gorelov, SFU)

Scientific motivation

The TRIUMF neutral atom trap (TRINAT) collaboration has pioneered the direct measurement of β^+–ν angular distributions by measuring the momentum of the few 100 eV energy recoiling nucleus in coincidence with the positron.

We have published the result of Expt. 715, the best measurement of a pure Fermi β–ν correlation parameter $a = 0.9981 \pm 0.0030 \pm 0.0037$ [Gorelov, Phys. Rev. Lett. **94**, 142501 (2005)], which is in agreement with the standard model prediction $a = 1$. These are the best limits on general scalar interactions coupling to the first generation of particles. The TRIUMF EEC in December, 2005 approved Expt. 1070, our proposal to improve the overall accuracy of this β–ν correlation experiment by a factor of 3. We also plan to extend the measurement to lower β energy to improve sensitivity to the scalar-vector Fierz interference term and hence gain better sensitivity to certain types of scalars, reaching accuracy directly competitive with the Q-value dependence of $0^+ \rightarrow 0^+$ ft values.

Figure 1 shows present limits on scalar interactions from our Expt. 715, the ft value experiments, and from the $\pi \rightarrow e\nu$ branching ratio in an effective field theory analysis [Campbell, Nucl. Phys. **B709**, 419 (2005)]. Here we have included the possibility of imaginary scalar couplings, which do not significantly change the result from Expt. 715 but have more impact on the other two types of experiments.

Scalars from SUSY Ramsey-Musolf has worked out the contribution of SUSY to first-generation interactions. If 0.001 accuracy can be achieved in the Fierz interference term, SUSY's assumption of couplings being small in the first generation can be meaningfully constrained [Ramsey-Musolf, nucl-th/0608035]. This provides additional motivation to extend our sensitivity to the lowest β energies, as the Fierz term scales with $1/E_\beta$.

Design progress and Expt. 1127

A great deal of design thought has gone into the very low-energy recoil-electron coincidence spectrometer needed for the isomer decay experiment (see Expt. 1127, this Annual Report). Much of this is directly relevant to the precision required in Expt. 1070 and to the measurement of potential backgrounds.

The time-focusing techniques considered for Expt. 1127 are under consideration here. If an extra drift space is included, then zero-velocity decays originating from anywhere in the trap can arrive at the MCP simultaneously. That would improve the precision of testing the electric field value from the fastest recoils by improving the time resolution. Designs that require grids are problematic because of the possible distortion of trajectories near the wires. Designs that enable time-focusing without grids are still under consideration.

A powerful feature of Expt. 1127 is its detection of monoenergetic recoils. This would test field configurations and explore backgrounds similar to the next round of precision β-ν correlation experiments in Expt. 1070. For example, the monoenergetic recoils produced would provide a powerful probe of possible backgrounds in those experiments for atoms from the walls and from molecular dimer formation. They would also provide precision tests of the electric field uniformity and value.

There are limitations to the Expt. 715 count rate from the resistive anode readout of MCP position information, as well as from CAMAC ADC readout. Our Expts. 1070 and 1127 upgrades plan to use delay line anode technology. We are also looking into moving our data acquistion to VME to take advantage, e.g., of an ASIC/FPGA based TDC developed at TRIUMF which is a clock-based system (our present TDC is based on charging/discharging a capacitor and has finite conversion time).

Electrostatic calculations In Expt. 715 we had a discrepancy between an electric field measured to be 807 ± 1 V/cm by three different experimental methods, and an electrostatic relaxation code's result of

800 V/cm. We have now shown that the relaxation code, which had a small mesh size everywhere because of the complexity of the electrodes, was not converging to sufficient accuracy. Earlier checks against the two-dimensional POISSON code were consistent, but the 2D geometries were necessarily simpler and did not test the fine mesh. SIMION and FEMLAB 3D calculations use additional or other methods and agree on the 807 V/cm value. This does not affect the Expt. 715 result as the experimentally determined field and error was used in the analysis, but it is likely that this new understanding will reduce a significant source of systematic error for Expt. 1070. This has been a major bottleneck in confidence in our designs and it is good to have overcome it.

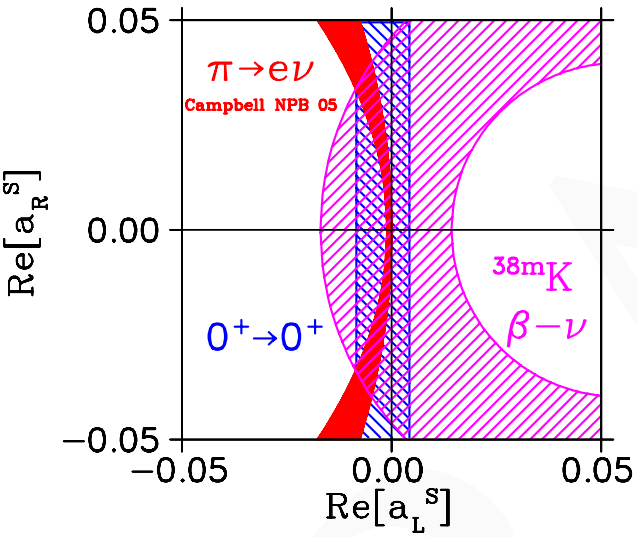

Fig. 1. Allowed combinations at 2σ of first-generation scalar interactions from three experiments. a_L^S is the scalar coupling to left-handed neutrinos, while a_R^S is the coupling to non-standard model right-handed neutrinos and is more strongly constrained by β-ν correlations.

Experiment 1127
Search for exotic particle emission in the decay of trapped isomers
(J.A. Behr, C. Höhr, TRIUMF)

Scientific motivation

We plan to measure the momentum of monoenergetic recoils from isomer γ decay using TRIUMF's neutral atom trap (TRINAT). This would make it possible to search for massive particles emitted by the nuclear transition instead of γ-rays. The recoiling nucleus would have lower momentum $p_x = \sqrt{E_\gamma^2 - m_x^2}$, producing a lower-momentum peak (see Fig. 1). This method does not rely on any information about interaction of the particles in any detector, and is independent of the lifetime of the particle.

Angular momentum selection rules favour production of spin and parity 0^- particles in transitions with magnetic multipolarity and 0^+ particles in electric transitions. We could also spin-polarize the isomers and measure angular distributions to determine the multipolarity of the emitted particle. Table I lists trappable isomers of Rb and Cs. We have explored motivation for such "signature-based searches" by considering possible 0^+ and 0^- particles that we could produce.

0^+ scalar particles Annihiliation of scalar particles with mass between 0.511 and 3 MeV into e^+-e^- pairs has been proposed to explain an observed spheroidal distribution of 511 keV γ-rays surrounding the galactic centre [Beacom, Phys. Rev. Lett. **97**, 071102 (2006)]. The 511s do not track the luminous matter distribution, so the scalar would also be a dark matter candidate. The decay of the 556 keV 6^- ^{86m}Rb isomer has sensitivity to part of this mass range (^{135m}Cs would extend that range). This model needs a new spin-1 exchange boson to mediate the interaction between the scalars, and we can also search for these.

0^- pseudoscalar particles A spontaneously broken global U(1) symmetry produces a pseudoscalar particle as a "pseudo-Goldstone boson". Such a symmetry has been suggested to explain the smallness of the CP-violating θ-term in QCD. Choosing the electroweak scale as the symmetry-breaking scale predicted "axion" masses of hundreds of keV and couplings in some models large enough to be seen in nuclear decays. Such large couplings were quickly ruled out in a variety of experiments, and attention shifted to a higher symmetry-breaking scale and m_{axion} <<1 eV, involving microwave cavities [Particle Data Group, J. Phys. **G33**, 1 (2006)], which our experment does not address. Models do exist for axions in the present considered mass range with smaller couplings that could still solve the strong CP problem. Our goal is to improve upon the best model-independent limits of $<2 \times 10^{-6}$ achieved in the decay of ^{139}La [Minowa, Phys. Rev. Lett. **71**, 4120 (1993)].

A model with a broken global U(1) symmetry to explain completely different physics, the size of the μ term in SUSY, predicts 0^- particles with masses and smaller couplings [Hall, Phys. Rev. **D70**, 115001 (2004)] which could be constrained by the present experiment.

Experimental geometry

For Expt. 956 we developed a geometry with back-to-back microchannel plates with a uniform electric field, one MCP to detect positive ions and the other to detect electrons. The natural background rate in each detector is about 10 Hz, and there is no evidence for electrons from field emission triggering the elec-

tron MCP. So we have considered other experiments that could take advantage of such a geometry and low background level.

A possible geometry for Expt. 1127 is sketched in Fig. 2.

Resonant photoionization The recoil is a neutral atom with energy less than 1 eV, so it will not fire a MCP. However, the recoil velocity of ∼1 mm/μs makes resonant photoionization practical.

We would excite the two-photon 778 nm 5S→5D transition in Rb. This transition is enhanced by the nearby 780 nm 5S→5P resonance, and can be saturated by a Ti:Sa ring with a 2 mm diameter beam. A 60 W 800 nm diode laser bar would then ionize the 5D at a rate of ∼10% per μs. (Similarly, the 6S→5D two-photon transition in Cs is enhanced by the nearby 6S→6P resonance.) In all cases we would use the coincidence with the photoelectron to measure the photoion TOF. In the case of 2-γ cascades (e.g. ^{84m}Rb), we would also use as a trigger either γ.

The hyperfine splittings of the isomers and ground states are different by more than 1 GHz. So the recoil can be resolved from the trapped isomer with selectivity better than 10^{-7} to 10^{-8}, which avoids unwanted background in the detectors and preserves the MOT lifetime.

γ-ray detection A γ-ray array with typical PET spatial resolution would allow searches in two-γ cascades (see Table I). One γ would be detected with high spatial and thus momentum resolution, serving as an additional trigger to discriminate against backgrounds. LADD is combining a $LaBr_3$(Ce) scintillator with a position-sensitive phototube for liquid xenon TPC tests, and this detector should be ideal. The critical requirements are timing and spatial resolution. If the γ is misidentified by its energy, it produces a higher reconstructed momentum which is not a background.

Time focusing and other improvements The geometry of Fig. 2 uses "time focusing". After acceleration in a uniform electric field, the ions are allowed to drift in a region of zero electric field. Decays originating from different positions in space will then arrive at the same time, greatly improving the time resolution and hence the overall momentum resolution, which is otherwise limited by the finite MOT size.

The geometry shown suggests a mesh to delineate the regions of different fields, though this has the disadvantage of deflecting the small percentage of ion trajectories that come very close to the wires. Geometries using no mesh and still providing time focusing are under consideration. Momentum focusing in the perpendicular direction is also being considered. A wide variety of such creative geometries have been used in atomic experiments at similar energies [Ullrich, Rep. Prog. Phys. **66**, 1463 (2003)].

2 photon emission Any single γ-ray transition can in principle emit two γs instead. The resulting three-body decay produces a continuous distribution of γ-ray energies that reflects their multipolarity and, if the initial nucleus is polarized, their angular distribution. This phenomenon has only been measured in ^{16}O, ^{40}Ca, and ^{90}Zr [Kramp, Nucl. Phys. **A474**, 412 (1987)].

If this effect occurs in our case, it would produce a continuous non-constant background that could limit the sensitivity to massive particles. It could then become an interesting signal in its own right.

The 2-photon nuclear transition goes by virtual excitation of all intermediate states. It is in that sense a possibly unique analogue of double β decay [Krmpotić, nucl-th/0601007] and might be useful as a test of the nuclear structure calculations needed for its interpretation. ^{130}Cs is the intermediate nucleus in a geochemical 2-ν double β decay, and similarly ^{86m}Rb could be useful. The isomer in ^{136}Cs would be most interesting, as ^{136}Xe neutrinoless double β decay is under active development, though little is known about it.

Summary In summary, our proposed technique is unique to atom traps and would measure the mass and coupling of any "invisible" particle produced in nuclear decays, with projected very small backgrounds. We would eventually determine the spin from the angular distribution of polarized decays. The experiments are tractable with small amounts of beam time taking advantage of the very large Rb yields demonstrated at ISAC.

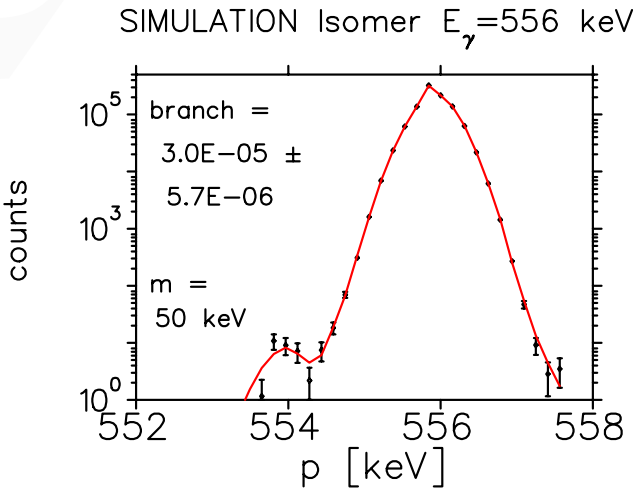

Fig. 1. Simulation of the momentum spectrum for the daughter nucleus momentum for the single γ-decay of ^{86m}Rb, including a hypothetical small branch for a massive particle producing a lower final nucleus momentum.

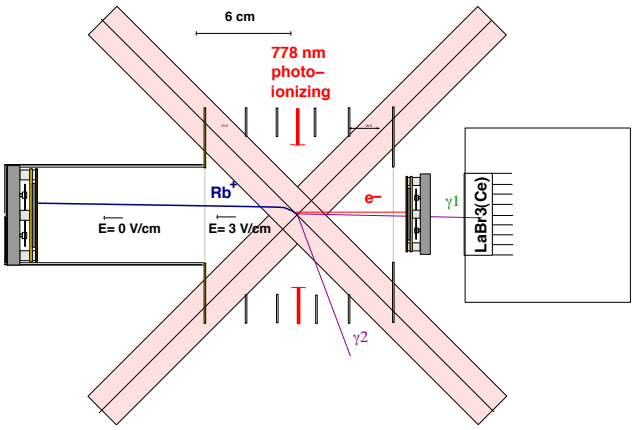

Fig. 2. Sketch of experimental geometry. The ion MCP is set back by a drift space for time focusing (see text).

Table I. Possible Rb and Cs isomers to trap. Listed are half-lives, number of γs in cascade, (main) γ-ray multipolarity, E_γ, and mass range explored. In one day of counting we would be sensitive to branching ratios of less than 2×10^{-6} in each case: the sensitivities listed ignore accidental coincidences.

$t_{1/2}$		# γ	M E	E_γ keV	m keV	Sens. /day $\times 10^{-6}$
20 m	^{84m}**Rb**	2	M3	216	100–160	2.0
4.3 m	^{90m}**Rb**	1	M3	107	20–85	2.1
2.9 m	^{138m}Cs	1	M3	80	15–60	2.8
3.5 m	^{130m}Cs	2	M1	83	60–80	0.5
		2	M3	15	10–13	0.2
2.9 h	^{134m}Cs	2	M1	11	6–8	0.6
53 m	^{135m}Cs	2	M4	846	400–800	0.6
		2	E2	787	400–750	0.6
1.0 m	^{86m}**Rb**	1	E4	556	40–400	0.05
					>511	50
31 m	^{81m}**Rb**	1	E3	86	20–80	0.2
19 s	^{136m}Cs	1	E3?	?	?	1

LANSCE Experiment NPDGamma Measurement of the parity-violating gamma asymmetry A_γ in the capture of polarized cold neutrons by para-hydrogen, $\vec{n} + p \rightarrow d + \gamma$

(S.A. Page, W.D. Ramsay, Manitoba)

Progress summary

Since the last Annual Report, the liquid hydrogen target has been installed in the NPDGamma cave on flight path 12 (FP12). All parts of the experiment are now commissioned and some data have been taken with liquid hydrogen. The target was first filled with liquid hydrogen in July. Prior to that, measurements of the parity violating γ-ray asymmetry were made on a wide range of nuclear targets. A paper based on these measurements has been published [Gericke *et al.*, Phys. Rev. **C74**, 065503 (2006)].

Background

The experiment is designed to measure the very slight, parity-violating, up-down γ-ray asymmetry, A_γ, in the radiative capture of vertically polarized cold neutrons on liquid para-hydrogen. A_γ provides a very clean measure of the weak pion-nucleon coupling, f_π^1. To a very good approximation, $A_\gamma = -0.11 f_\pi^1$. Existing experimental data appear to disagree on the value of f_π^1. The circular polarization of 1081 keV γ-rays from ^{18}F apparently restricts f_π^1 to $0 \pm 1 \times 10^{-7}$, while the ^{133}Cs anapole moment implies $f_\pi^1 = 7 \pm 3 \times 10^{-7}$. Because the NPDGamma experiment is based on a simple two-nucleon system without the complex many-body dynamics of the ^{18}F and ^{133}Cs experiments, we expect it to produce a definitive result. The original goal was to measure f_π^1 to $\pm 0.5 \times 10^{-7}$, corresponding to a precision of $\pm 0.5 \times 10^{-8}$ in A_γ. Unfortunately, the beam intensity and moderator brightness at LANSCE were each approximately half what was expected, and interference from a neighbouring flight path reduced the possible running time per year by one-half. As a result, following the 2006 run at Los Alamos during which it was determined that the equipment worked as expected and that systematic errors were under control, the experiment is now being dismantled and will be moved to the Spallation Neutron Source (SNS) at Oak Ridge. Once the apparatus is commissioned at the SNS, it should be possible to measure A_γ to a statistical precision of $\pm 1 \times 10^{-8}$ in 4000 hours at the design power of 1.4 MW. The mid-range theoretical prediction for A_γ is -5×10^{-8}.

Experimental overview

An overview of the $np \rightarrow d\gamma$ experiment is shown in Fig. 1. A 20 Hz pulsed beam of cold neutrons is transported to the experiment through an m = 3 supermirror neutron guide and enters the experimental cave. The cave is shown in Fig. 1 with the roof removed to reveal the equipment. The neutrons are polarized by a ^{3}He spin filter in a uniform 10 G vertical guide field, which is constant over the entire experiment. The vertically polarized neutrons are then captured in liquid hydrogen with the emission of 2.2 MeV γ-rays. The 100 kPa, 17 K liquid hydrogen target achieves an equilibrium composition of 99.8% para-hydrogen, which prevents spin flip scattering and the consequent neutron depolarization which would occur with ortho-hydrogen. To reduce systematic error, an rf spin flipper reverses the neutron spins at the 20 Hz neutron frame rate. Capture gammas are detected in an array of 48 CsI(Tl) crystals. Three beam monitors, which were provided by the Manitoba group, are used to determine the neutron polarization and to monitor the para/ortho hydrogen ratio in the target.

Determining effective detector locations

Capture γ-rays are detected by an array of 48 CsI cubes arranged around the liquid hydrogen target as shown in Fig. 2. If the detector array is not accurately aligned, some parity allowed left-right asymmetry can appear as a false parity violating up-down signal. To keep false asymmetry from this source below 5×10^{-10}, the effective position of each of the 48 CsI cells must be known to 20 mrad. Measuring the physical position is not sufficient as there is no guarantee that the detector response is uniform throughout a cube. To determine the *effective* positions, the yield from each CsI cell is measured as the detector array is moved relative to the target. The effective positions are then calculated from these data. The position scanning is done using a computer controlled precision motion system developed and installed by the Canadian Manitoba/TRIUMF group.

Figure 3 shows results of such a scan with a Cd target in place. The data are for the twelve detectors of ring 2. The outer plots show the yield as a function of detector position over 25 positions on a 5×5 grid. The step size is 4 mm. The centre plot shows the calculated position of each cell. The resolution obtained was 5.6 mm in x and 2.8 mm in y. During production running, this same procedure is used with the liquid hydrogen target in place.

During the last year, collaborators from TRIUMF have made improvements to the motion control software. For example, better absolute homing capability was added. The routines make use of the system's absolute position encoders to bring the array back to a known surveyed position. Figure 4 shows a screen capture of the updated motion control interface.

Nuclear target measurements

A very productive part of the past year has been the measurement of parity violating asymmetries in the radiative capture of cold neutrons on a variety of nuclear targets. Targets of Al, Mn, Co, Sc, Ti, Mn, In, V, Pb, Cu, and stainless steel have been used. The results have an immediate practical use because some of the target materials are present in the beam line and knowledge of the parity violating asymmetries from these materials gives us better control of systematic errors. In addition, may of the asymmetries in this mass range have not been measured before and are of scientific interest in their own right. The results form the basis of the Ph.D. thesis of Mikayel Dabaghyan and of a paper published in Physical Review C [Gericke *et al., op. cit.*].

The properties of the most desirable targets from a scientific standpoint include

- Large neutron capture cross section for high statistics;
- Small scattering cross section for low background;
- Small incoherent cross section to minimize depolarization;
- Close level spacing with mixing of opposite-parity states to give large asymmetry.

Table I shows some preliminary results for a variety of targets. Not all data have been analyzed for every target. Note that a null test using LEDs gave $(-2.0 \pm 1.1) \times 10^{-8}$, confirming that false asymmetry from electronic sources is not significant compared to the statistical uncertainties.

Liquid hydrogen target

The target contains 20 L of liquid para-hydrogen in a 30 cm long vessel. According to simulations, this thickness will absorb about 60% of the neutron beam. During summer, 2005, off-line tests of the target were conducted in a test shed at the Lujan Center. The target could not be installed in the FP-12 cave until the hydrogen vent lines were in place and the target had passed the appropriate safety reviews. The vent lines to the cave were completed in August, 2005, and safety approval was finally received in March, 2006, at which time the target was moved to the FP12 cave (Fig. 5). After a series of empty-target tests in the cave, final approval to run liquid hydrogen was received in July. During July and August, the first liquid hydrogen tests were made. Once the target is full, production data cannot be taken until the ortho/para conversion is complete. Figure 6 shows the para-hydrogen fraction measured over a few days in August. The final concentration was 99.82% para-hydrogen.

Liquid hydrogen target measurements

Liquid hydrogen running began in August. Figure 7 shows up-down asymmetries measured once the conversion to para-hydrogen had completed. The statistics indicate that $\pm 1 \times 10^{-7}$ should be achievable in 80 days of steady running.

Neutron beam and ^{3}He polarization

Neutrons for the NPDGamma experiment are polarized by passing the neutron beam through a cell containing polarized ^{3}He. Because the capture cross section is strongly dependent on the spin direction (2 barns parallel compared to 17,000 barns anti-parallel at 10 meV, and increasing at lower energy), neutrons with the "wrong" spin are filtered out, leaving the beam polarized. The increase in capture cross section for slower neutrons means that the neutron polarization varies across each data-taking "frame", with the highest polarization for the slow neutrons arriving at

the end of the interval. Perhaps surprisingly, the neutron beam polarization can be calculated by simply measuring the transmission through the ^{3}He cell in its polarized and unpolarized states. It is not necessary to know the ^{3}He polarization. If T_0 is the transmission through the unpolarized cell, and T is the transmission through the polarized cell, then the neutron beam polarization when the cell is polarized is $P_n = \sqrt{1-(\frac{T_0}{T})^2}$. Once the neutron beam polarization is known, the ^{3}He polarization may be calculated from $P_n = \tanh(n\sigma l P_3)$, where n is the number density of ^{3}He, σ is the capture cross section, l is the thickness of the cell, and P_3 is the ^{3}He polarization. The neutron polarization can be higher than the ^{3}He polarization. Figure 8 shows the neutron polarization for a series of runs. The values are averages over all active time bins. The error bars shown are dominated by uncertainties in pedestals and background so the points show less scatter than would be expected if the uncertainties were statistics dominated.

Collaborators: R. Alarcon, L. Baron (Arizona State); J.D. Bowman, G.S. Mitchell, S.I. Penttila, W.S. Wilburn, V.W. Yuan (Los Alamos National Lab); R.D. Carlini (Jefferson Lab); W. Chen (Indiana/NIST); T.E. Chupp, M. Sharma (Michigan); C. Crawford, R. Mahurin (Tennessee); S. Covrig, M. Dabaghyan, F.W. Hersman (New Hampshire); S.J. Freedman, B. Lauss (California, Berkeley); T.R. Gentile (NIST); M. Gericke, R.C. Gillis, S.A. Page (Manitoba); G.L. Greene (Tennessee/Oak Ridge Nat. Lab); T. Ino, Y. Masuda, S. Muto (KEK); G.L. Jones (Hamilton College); M.B. Leuschner, B. Losowski, J. Mei, H. Nann, W.M. Snow (Indiana); W.D. Ramsay (Manitoba/TRIUMF); S. Santra (Bhabha Atomic Research Center); P.-N. Seo (North Carolina State); E.I. Sharapov (JINR Dubna); T.B. Smith (Dayton).

Table I. Preliminary up-down asymmetries.

Target	A_γ
Al	$(-0.02 \pm 3) \times 10^{-7}$
Cl	$(-21 \pm 1.6) \times 10^{-6}$
B_4C	$(-1 \pm 2) \times 10^{-6}$
Co	$(6.1 \pm 3.1) \times 10^{-7}$
Cu	$(-1 \pm 3) \times 10^{-6}$
In	$(-6.8 \pm 3) \times 10^{-7}$
Mn	$(5.3 \pm 7.8) \times 10^{-7}$
Sc	$(-10.4 \pm 2.5) \times 10^{-7}$
Ti	$(4.1 \pm 3.6) \times 10^{-7}$
V	$(2.4 \pm 4.5) \times 10^{-7}$

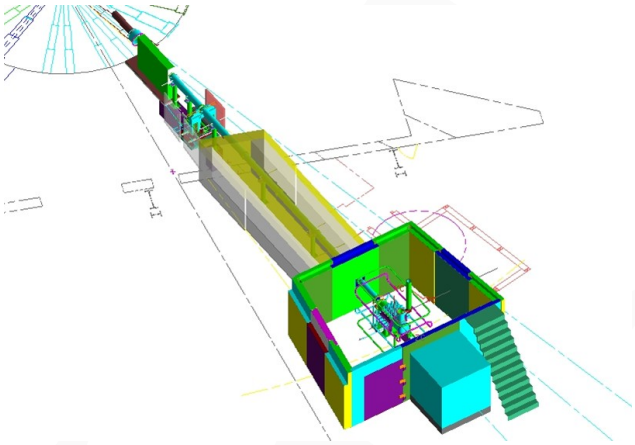

Fig. 1. The NPDGamma experiment shown in the cave on flight path 12 (FP12) at LANSCE.

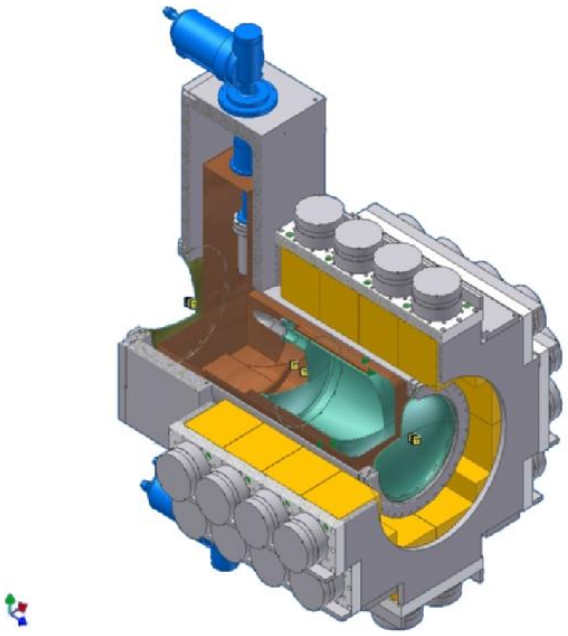

Fig. 2. Arrangement of the detector array around the liquid hydrogen target. The array comprises 48 150×150×150 mm^3 cubes of CsI. To determine the effective centre of each CsI cube, the whole array is moved and the cube positions are calculated from the variations in yield with position. The motion is accomplished by a computer controlled precision motion system developed and built by the Manitoba/TRIUMF group.

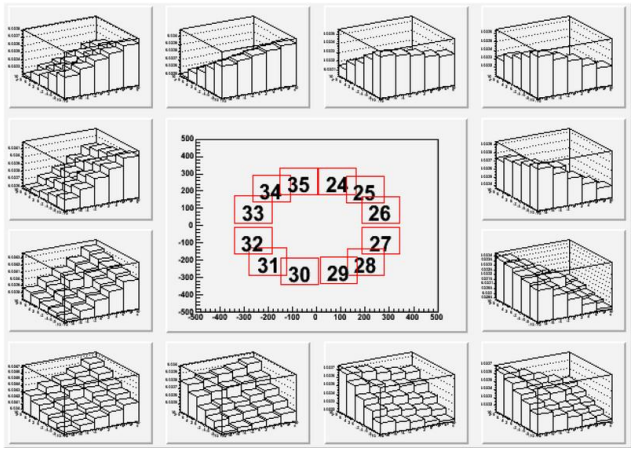

Fig. 3 Detector cell yields vs. array position for one ring of the CsI array. The outer plots show the variation in yield as the array was scanned in 4 mm steps over a 5×5 grid in x and y. The central diagram shows the cell positions calculated from the variation in yield with position.

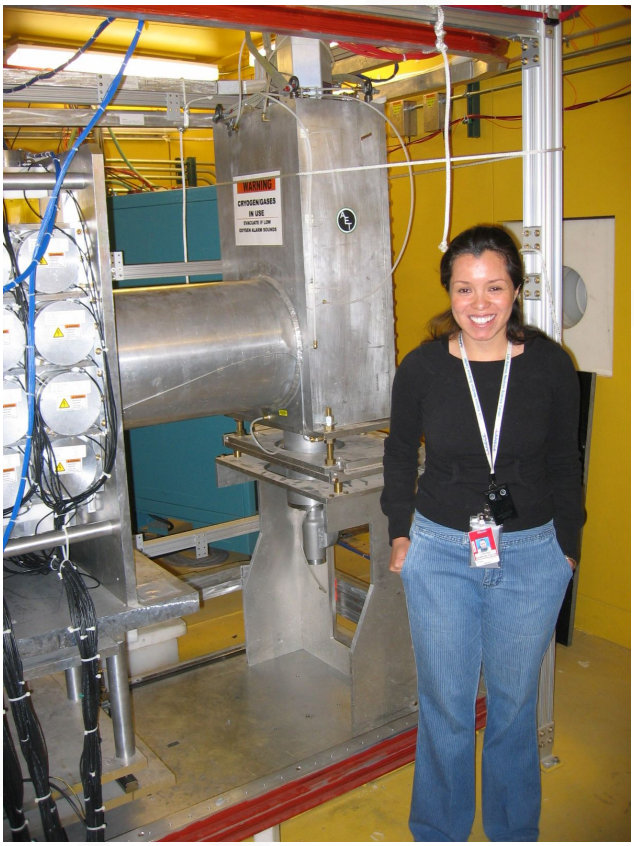

Fig. 5. Liquid hydrogen target in the FP12 cave. The target was moved from the test shed to the cave in March. The first operation with liquid hydrogen on FP12 was in July.

Fig. 4 Updated control interface for the TRIUMF motion control system. Several upgrades were made to this system in 2006.

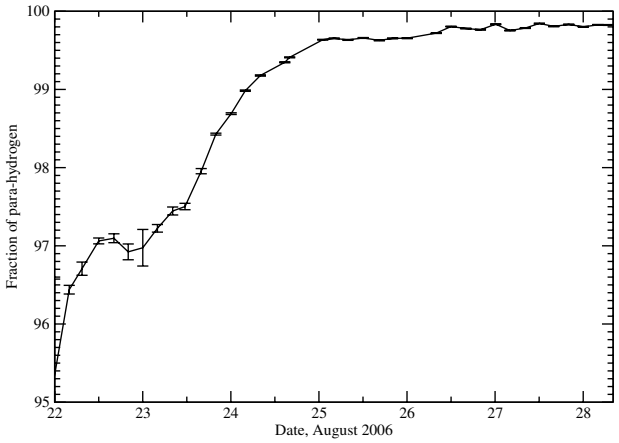

Fig. 6. Para-hydrogen fraction measured during August. The final concentration is 99.82%, suitable for production data-taking.

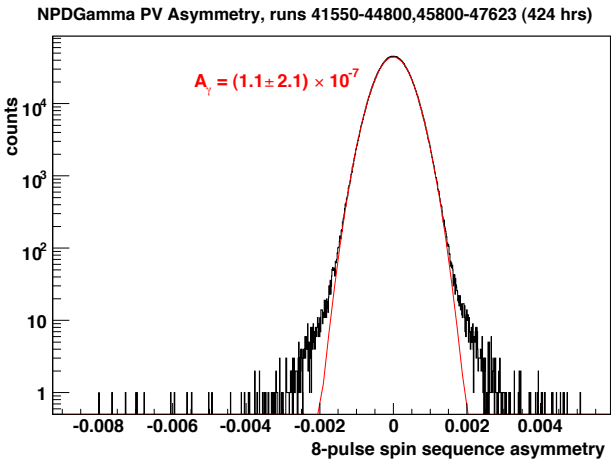

Fig. 7. Up-down asymmetries for 8-spin-state sequences representing 424 hours of running on para-hydrogen. The statistics indicate we should achieve $\pm 1 \times 10^{-7}$ in 80 days of steady running. The non-Gaussian tails are from octets with low beam current.

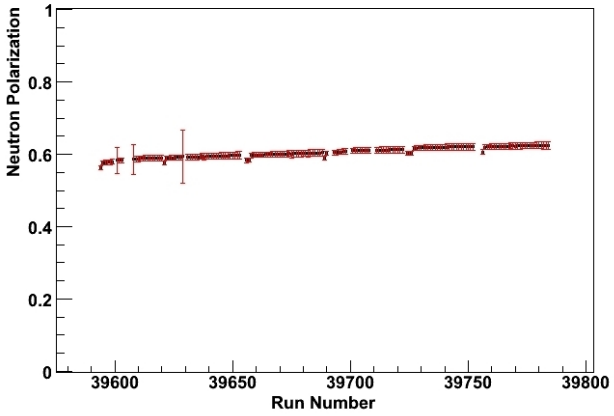

Fig. 8. Neutron polarization for a series of runs. The values are averages over all times of flight and frames in a run.